INTERNATIONAL JOURNAL FOR NUMERICAL METHODS IN ENGINEERING
Int. J. Numer. Meth. Engng 2011; **87**:1278–1300
Published online 23 February 2011 in Wiley Online Library (wileyonlinelibrary.com). DOI: 10.1002/nme.3159

A large deformation frictional contact formulation using NURBS-based isogeometric analysis

L. De Lorenzis[1,*,†], İ. Temizer[2], P. Wriggers[3] and G. Zavarise[1]

[1]*Department of Innovation Engineering, University of Salento, Lecce, Italy*
[2]*Department of Mechanical Engineering, Bilkent University, Bilkent, Ankara, Turkey*
[3]*Institut für Kontinuumsmechanik, Leibniz Universität Hannover, Hannover, Germany*

SUMMARY

This paper focuses on the application of NURBS-based isogeometric analysis to Coulomb frictional contact problems between deformable bodies, in the context of large deformations. A mortar-based approach is presented to treat the contact constraints, whereby the discretization of the continuum is performed with arbitrary order NURBS, as well as C^0-continuous Lagrange polynomial elements for comparison purposes. The numerical examples show that the proposed contact formulation in conjunction with the NURBS discretization delivers accurate and robust predictions. Results of lower quality are obtained from the Lagrange discretization, as well as from a different contact formulation based on the enforcement of the contact constraints at every integration point on the contact surface. Copyright © 2011 John Wiley & Sons, Ltd.

Received 11 October 2010; Revised 5 January 2011; Accepted 10 January 2011

KEY WORDS: contact mechanics; isogeometric analysis; NURBS; mortar method

1. INTRODUCTION

Isogeometric analysis, recently presented by Hughes *et al.* [1], can be regarded as a successful merging of computer-aided design and the finite element method (FEM). In the last few years this new computational mechanics technology has been successfully applied to a variety of problems [2–7].

The potential of isogeometric analysis for contact modeling was already suggested in the original paper by Hughes *et al.* [1]. As NURBS geometries can attain the desired degree of continuity at the element boundaries, they possess the premises to alleviate all the problems arising particularly in sliding contact when using conventional Lagrange polynomial elements, which are only C^0-continuous at the interelement nodes. Such problems have often been faced by introducing smoothing techniques [8–12], some of which involve NURBS interpolation [13, 14]. These procedures generally improve the performance of the contact algorithms by enhancing the continuity of the contact surfaces, however they do not increase the order of convergence as the higher order approximation does not involve the bulk behavior of the solids. Temizer *et al.* [15] applied NURBS-based isogeometric analysis to thermomechanical frictionless contact problems. Qualitative analyses on large deformation frictionless sliding indicated a superior iterative convergence behavior of NURBS discretizations over Lagrange ones. The analysis of the classical Hertz problem demonstrated the superiority of the NURBS discretization in terms of quality and robustness of

*Correspondence to: L. De Lorenzis, Department of Innovation Engineering, University of Salento, Lecce, Italy.
†E-mail: laura.delorenzis@unisalento.it

results. It was also pointed out that the enforcement of the contact constraints at each Gauss point on the contact surfaces delivers unstable results, and therefore a mortar-based formulation must be pursued.

In this paper, NURBS-based isogeometric analysis is adopted to model 2D large deformation Coulomb frictional contact problems. Section 2 describes the formulation of the contact problem using the penalty method for both frictionless and frictional conditions. Section 3 illustrates the NURBS discretization. Sections 4 and 5 present the contact formulation in detail, up to the full linearization which is deferred to the Appendix. Finally, in Section 6 some numerical examples are presented and their results are compared and discussed.

2. LARGE DEFORMATION CONTACT PROBLEM

This section summarizes the theoretical and algorithmic background of the contact between two deformable bodies undergoing finite deformations, for more details see Laursen [16] and Wriggers [17].

2.1. Problem description

Two 2D elastic bodies are assumed to come into contact undergoing large deformations. The bodies are denoted as slave (or non-mortar), B^{s}, and master (or mortar), B^{m}. The relation between the initial (reference) configuration $\mathbf{X}$, the displacement $\mathbf{u}$, and the current configuration $\mathbf{x}$ of the generic point of each body is given by

$$\mathbf{x}^i = \mathbf{X}^i + \mathbf{u}^i \tag{1}$$

where the superscript $i = \{s, m\}$ denotes, respectively, the slave and master bodies.

The master surface is parameterized via the convective coordinate ξ that defines the covariant vector $\boldsymbol{\tau}_1 = \mathbf{x}^{\mathrm{m}}_{,\xi}$. Using the metric $m_{11} := \boldsymbol{\tau}_1 \cdot \boldsymbol{\tau}_1$ with inverse component m^{11}, the contravariant vector $\boldsymbol{\tau}^1 := m^{11}\boldsymbol{\tau}_1$ is induced. The curvature follows from $k_{11} = \mathbf{x}^{\mathrm{m}}_{,\xi\xi} \cdot \mathbf{n}$, where $\mathbf{n} = \mathbf{n}^{\mathrm{m}}$ is the normal unit vector.

In the current configuration, the contact interface is $\Gamma_{\mathrm{c}} := \Gamma^{\mathrm{s}}_{\mathrm{c}} = \Gamma^{\mathrm{m}}_{\mathrm{c}}$, Γ^i_{c} being the current contact boundary on body B^i. For its determination, a function is introduced which describes the distance between a given point of position $\mathbf{x}^{\mathrm{s}}$ on $\Gamma^{\mathrm{s}}_{\mathrm{c}}$ and an arbitrary point located at $\mathbf{x}^{\mathrm{m}} = \mathbf{x}^{\mathrm{m}}(\xi)$ on $\Gamma^{\mathrm{m}}_{\mathrm{c}}$

$$d := \| \mathbf{x}^{\mathrm{s}} - \mathbf{x}^{\mathrm{m}}(\xi) \| . \tag{2}$$

The projection of each point of the slave surface onto the master one is carried out by minimizing such distance. This closest point projection defines a residual

$$f(\xi) = \boldsymbol{\tau}_1(\xi) \cdot [\mathbf{x}^{\mathrm{s}} - \mathbf{x}^{\mathrm{m}}(\xi)] \tag{3}$$

that vanishes at the projection point corresponding to $\overline{\xi}$, i.e. $f(\overline{\xi}) = 0$. The iterative process starting from an initial guess $\hat{\xi}$ requires the tangent

$$K_{11} = f_{,\xi} = \mathbf{x}^{\mathrm{m}}_{,\xi\xi}(\xi) \cdot [\mathbf{x}^{\mathrm{s}} - \mathbf{x}^{\mathrm{m}}(\xi)] - m_{11}(\xi). \tag{4}$$

The closest projection point and the related variables are often identified in the literature with the $(\overline{\bullet})$ notation, such as $\overline{\mathbf{x}}^{\mathrm{m}} = \mathbf{x}^{\mathrm{m}}(\overline{\xi})$. In the following, to simplify the notation the bar will mostly be omitted, and all the quantities related to the master surface will be implicitly intended as evaluated at the projection point.

The contact interface is pulled back to $\Gamma_{\mathrm{c0}} := \Gamma^{\mathrm{s}}_{\mathrm{c0}} \neq \Gamma^{\mathrm{m}}_{\mathrm{c0}}$, where Γ^i_{c0} is the contact boundary in the reference configuration on body B^i. In the present formulation all contact integrals will be evaluated on $\Gamma^{\mathrm{s}}_{\mathrm{c0}}$. This has been shown to exert no appreciable influence on the results in most cases of interest [18].

DOI: 10.1002/nme

2.2. Contact variables and constraints

The normal gap, g_N, and the tangential slip increment, $\dot{\mathbf{g}}_T$, between the two bodies are defined as

$$g_N = (\mathbf{x}^{\mathrm{s}} - \overline{\mathbf{x}}^{\mathrm{m}}) \cdot \mathbf{n} \quad \dot{\mathbf{g}}_T = \dot{\overline{\xi}} \boldsymbol{\tau}_1. \tag{5}$$

Note that, with this definition, the gap is positive if the contact is open and negative when penetration of the bodies takes place. The tangential slip is often defined in incremental form, which is suitable for the time-discretized backward Euler formulation

$$\dot{\overline{\xi}} = (\overline{\xi} - \overline{\xi}_n)/\Delta t \longrightarrow \dot{\mathbf{g}}_T = (\mathbf{g}_T - \mathbf{g}_{T_n})/\Delta t = (\overline{\xi} - \overline{\xi}_n)/\Delta t \boldsymbol{\tau}_1. \tag{6}$$

Here and in the following, all quantities will refer by default to the current time step $t = t_{n+1}$, whereas the subscript n as in Equation (6) will be used to refer to the previous time step t_n.

The normal contact traction t_N and the tangential contact traction $\mathbf{t}_T$ are defined in terms of the Piola traction vector $\mathbf{t} = \mathbf{t}^{\mathrm{m}} = -\mathbf{t}^{\mathrm{s}}$, which is resolved into its normal and tangential components

$$\mathbf{t} = \mathbf{t}_N + \mathbf{t}_T = t_N \mathbf{n} + t_{T_1} \boldsymbol{\tau}^1 \quad t_N = \mathbf{t} \cdot \mathbf{n}. \tag{7}$$

Considering unilateral contact without adhesion, the Kuhn–Tucker conditions for impenetrability on Γ_{c0} are

$$g_N \geqslant 0, \quad t_N \leqslant 0, \quad g_N t_N = 0 \quad \dot{g}_N t_N = 0 \tag{8}$$

and the tangential contact constraints are obtained by combining the tangential slip increment and contact traction with the Kuhn–Tucker conditions for Coulomb friction

$$\Phi = \| \mathbf{t}_T \| - \mu t_N \leqslant 0 \quad \dot{\mathbf{g}}_T = \dot{\gamma} \frac{\mathbf{t}_T}{\| \mathbf{t}_T \|} \quad \gamma \geqslant 0 \quad \gamma \Phi = 0 \tag{9}$$

where μ is the coefficient of friction and γ is the amount of slip.

2.3. Penalty regularized contact constraints

The contact constraints introduced above are here regularized using the penalty method. The regularized normal contact constraint reads as

$$t_N = \varepsilon_N \langle g_N \rangle_- \quad \langle g_N \rangle_- = \begin{cases} g_N & \text{if } g_N \leqslant 0 \\ 0 & \text{otherwise} \end{cases} \tag{10}$$

where $\varepsilon_N > 0$ is the normal penalty parameter. In the tangential direction, the regularized friction constraint in the time-discretized setting (using Euler backward integration) takes the form

$$t_{T_1} = t_{T_{1n}} + \varepsilon_T \left[m_{11}(\overline{\xi} - \overline{\xi}_n) - \gamma \frac{t_{T_1}}{|t_{T_1}|} \right] \quad \Phi \leqslant 0 \quad \gamma \geqslant 0 \quad \Phi \gamma = 0 \tag{11}$$

where $\varepsilon_T > 0$ is the tangential penalty parameter and $\gamma = \dot{\gamma} \Delta t$ is the incremental plastic slip.

Application of the classical return mapping algorithm yields the following algorithmic update formula for the frictional traction. The trial state is first computed by assuming that $\gamma = 0$

$$t_{T_1}^{\mathrm{trial}} = t_{T_{1n}} + \varepsilon_T m_{11}(\overline{\xi} - \overline{\xi}_n) \quad \Phi^{\mathrm{trial}} = \| \mathbf{t}_T^{\mathrm{trial}} \| - \mu t_N \tag{12}$$

and the status of stick or slip is then determined based on

$$t_{T_1} = \begin{cases} t_{T_1}^{\mathrm{trial}} & \text{if } \Phi^{\mathrm{trial}} \leqslant 0 \\ -\mu t_N \dfrac{t_{T_1}^{\mathrm{trial}}}{\| \mathbf{t}_T^{\mathrm{trial}} \|} = -\mu \varepsilon_N g_N \dfrac{t_{T_1}^{\mathrm{trial}}}{\| \mathbf{t}_T^{\mathrm{trial}} \|} & \text{otherwise.} \end{cases} \tag{13}$$

DOI: 10.1002/nme

2.4. Variations and linearizations of the contact variables

The variations of the contact kinematical quantities are as follows, for details see e.g. [16] and [17],

$$\delta g_N = (\delta \mathbf{x}^{\mathrm{s}} - \delta \overline{\mathbf{x}}^{\mathrm{m}}) \cdot \mathbf{n} \quad \delta \mathbf{g}_T = \delta \overline{\xi} \boldsymbol{\tau}_1 \quad \delta \overline{\xi} = \frac{1}{m_{11} - g_N k_{11}} [(\delta \mathbf{x}^{\mathrm{s}} - \delta \overline{\mathbf{x}}^{\mathrm{m}}) \cdot \boldsymbol{\tau}_1 + g_N \mathbf{n} \cdot \delta \overline{\mathbf{x}}^{\mathrm{m}}_{,\xi}]. \tag{14}$$

The variation of the frictional traction derives from the presented time integration scheme. After some manipulations the variations of the tangential tractions are obtained as

$$\delta t_{T_1}^{\mathrm{trial}} = \varepsilon_T [m_{11} \delta \overline{\xi} + 2(\overline{\mathbf{x}}_{,\xi\xi} \cdot \boldsymbol{\tau}_1 \Delta \overline{\xi} + \Delta \overline{\mathbf{x}}_{,\xi} \cdot \boldsymbol{\tau}_1)(\overline{\xi} - \overline{\xi}_n)] \tag{15}$$

$$\delta t_{T_1} = -\mu \varepsilon_N \operatorname{sign}(t_{T_1}^{\mathrm{trial}}) \left[\sqrt{m_{11}} \delta g_N + \frac{g_N}{\sqrt{m_{11}}} (\overline{\mathbf{x}}_{,\xi\xi} \cdot \boldsymbol{\tau}_1 \Delta \overline{\xi} + \Delta \overline{\mathbf{x}}_{,\xi} \cdot \boldsymbol{\tau}_1) \right] \tag{16}$$

for the stick and slip cases, respectively. The linearized increments of all the above quantities are simply obtained by substituting the symbol for virtual variation, δ, with that for linearized increment, Δ.

Finally, the linearizations of the kinematical quantities are given by

$$\begin{aligned} \Delta \delta g_N = & -(\delta \overline{\mathbf{x}}^{\mathrm{m}}_{,\xi} \Delta \overline{\xi} + \Delta \overline{\mathbf{x}}^{\mathrm{m}}_{,\xi} \delta \overline{\xi} + \overline{\mathbf{x}}^{\mathrm{m}}_{,\xi\xi} \Delta \xi \delta \overline{\xi}) \cdot \mathbf{n} \\ & + \frac{g_N}{m_{11}} (\delta \overline{\mathbf{x}}^{\mathrm{m}}_{,\xi} + \overline{\mathbf{x}}^{\mathrm{m}}_{,\xi\xi} \delta \overline{\xi}) \mathbf{n} \otimes \mathbf{n} (\Delta \overline{\mathbf{x}}^{\mathrm{m}}_{,\xi} + \overline{\mathbf{x}}^{\mathrm{m}}_{,\xi\xi} \Delta \overline{\xi}) \end{aligned} \tag{17}$$

$$\begin{aligned} (m_{11} - g_N k_{11}) \Delta \delta \overline{\xi} = & -\boldsymbol{\tau}_1 \cdot (\delta \overline{\xi} \Delta \overline{\mathbf{x}}_{,\xi} + \delta \overline{\mathbf{x}}_{,\xi} \Delta \overline{\xi}) \\ & -(\boldsymbol{\tau}_1 \cdot \boldsymbol{\tau}_{1,\xi} - g_N \mathbf{n} \cdot \boldsymbol{\tau}_{1,\xi\xi}) \delta \overline{\xi} \Delta \overline{\xi} + g_N (\delta \overline{\xi} \Delta \overline{\mathbf{x}}_{,\xi\xi} + \delta \overline{\mathbf{x}}_{,\xi\xi} \Delta \overline{\xi}) \cdot \mathbf{n} \\ & -(\delta \overline{\mathbf{x}}_{,\xi} + \boldsymbol{\tau}_{1,\xi} \delta \overline{\xi}) \cdot \boldsymbol{\tau}_1 \Delta \overline{\xi} - (\Delta \overline{\mathbf{x}}_{,\xi} + \boldsymbol{\tau}_{1,\xi} \Delta \overline{\xi}) \cdot \boldsymbol{\tau}_1 \delta \overline{\xi} \\ & +(\mathbf{x}^{\mathrm{s}} - \overline{\mathbf{x}}^{\mathrm{m}}) \cdot (\Delta \overline{\mathbf{x}}_{,\xi} + \boldsymbol{\tau}_{1,\xi} \Delta \overline{\xi}) + (\Delta \mathbf{x}^{\mathrm{s}} - \Delta \overline{\mathbf{x}}^{\mathrm{m}}) \cdot (\delta \overline{\mathbf{x}}_{,\xi} + \boldsymbol{\tau}_{1,\xi} \delta \overline{\xi}). \end{aligned} \tag{18}$$

2.5. Contact virtual work

The contact contribution to the virtual work is given by

$$\delta W_{\mathrm{c}} = \int_{\Gamma_{\mathrm{c}0}} [t_N \delta g_N + t_{T_1} \delta \overline{\xi}] \, \mathrm{d}\Gamma. \tag{19}$$

Its linearization follows immediately as

$$\Delta \delta W_{\mathrm{c}} = \int_{\Gamma_{\mathrm{c}0}} [\Delta t_N \delta g_N + t_N \Delta \delta g_N + \Delta t_{T_1} \delta \overline{\xi} + t_{T_1} \Delta \delta \overline{\xi}] \, \mathrm{d}\Gamma \tag{20}$$

where all quantities, variations, and linearizations can be found in the previous section.

3. NURBS DISCRETIZATION

This section describes briefly the bivariate NURBS discretization used for the continuum and the ensuing univariate NURBS discretization of the contact surfaces. In what follows, standard NURBS terminology is employed. For further details and extensive references see Piegl and Tiller [19] and Cottrell *et al.* [6].

Let Ξ^i be the open non-uniform knot vector associated with the ith dimension of a patch, $i = \{1, 2\}$

$$\Xi^i = \{\xi_1^i, \ldots, \xi_{n_i + p_i + 1}^i\}. \tag{21}$$

DOI: 10.1002/nme

The first p_i+1 terms in Ξ^i are equal, and so are the last p_i+1 terms. Here, p_i are the polynomial orders of the accompanying B-spline basis functions, ξ^i_j is the jth knot and n_i is the number of accompanying control points in the ith dimension. If Ξ^i has no repeated interior knot ξ^i_j, $j\in[p_i+1,n_i]$, the number of non-zero interior knot spans is n_i-p_i, and this corresponds to the number of elements in the same dimension. Every repetition of an interior knot decreases the number of elements by one. A surface is parameterized by

$$\mathbf{S}(\xi^1,\xi^2)=\sum_{d_1=1}^{n_1}\sum_{d_2=1}^{n_2}R_{d_1d_2}(\xi^1,\xi^2)\mathbf{X}_{d_1d_2} \tag{22}$$

where $\mathbf{X}_{d_1d_2}$ are the control point coordinates and $R_{d_1d_2}\geqslant 0$ are the rational B-spline (NURBS) basis functions. The latter are defined via a tensor product in a three-dimensional space based on homogeneous coordinates [19]. The projected form in the two-dimensional space is

$$R_{d_1d_2}(\xi^1,\xi^2)=\frac{w_{d_1d_2}}{W(\xi^1,\xi^2)}B^1_{d_1}(\xi^1)B^2_{d_2}(\xi^2) \tag{23}$$

with $B^i_{d_i}$ as a piecewise polynomial B-spline basis function. The normalizing weight W is given in terms of the weights $w_{d_1d_2}$ and of the functions $B^i_{d_i}$ via

$$W(\xi^1,\xi^2)=\sum_{d_1=1}^{n_1}\sum_{d_2=1}^{n_2}w_{d_1d_2}B^1_{d_1}(\xi^1)B^2_{d_2}(\xi^2). \tag{24}$$

The knot vectors together with the associated control points and the accompanying weights constitute a patch. The continuity and order of $B^i_{d_i}$ depends on Ξ^i only. If Ξ^i has no repeated interior knot ξ^i_j, $j\in[p_i+1,n_i]$, then the order-p_i basis function $B^i_{d_i}$ has continuity C^{p_i-1}. Every repetition of a knot decreases the continuity by one order at this knot. The order of NURBS parameterization will be denoted by N^p in subsequent sections, while the order of Lagrange polynomials employed will be denoted by L^p.

The counterparts of the h- and p-refinement procedures for FEM discretizations based on Lagrange polynomials are the knot insertion and order elevation procedures in the NURBS setting. While p-refinement for Lagrange discretizations preserves the number of nodes, order elevation for NURBS leads to a slight increase in the number of control points. When knot insertion and order elevation must be conducted together, the k-refinement procedure will be employed where knot insertion precedes order elevation [6]. This has the advantage that a higher degree of smoothness can be achieved within the patch across non-repeated knot entries and the final number of control points is less compared to the case where knot refinement precedes. For the numerical evaluation of the weak forms emanating from Lagrange or NURBS-based discretizations, $2p$ Gauss–Legendre quadrature points will be employed within each element for order-p approximations. This ensures a converged quadrature. See Hughes *et al.* [20] for a recent discussion of efficient quadrature schemes appropriate for isogeometric analysis.

The contact discretized surface is a univariate NURBS curve that is directly inherited from the bivariate NURBS surface discretization. For instance, let $\xi^1_-:=\xi^1_1$. By construction [19]

$$\mathbf{S}(\xi^1_-,\xi^2)=\sum_{d_2=1}^{n_2}R^-_{d_2}(\xi^2)\mathbf{X}^-_{d_2} \tag{25}$$

where $\mathbf{X}^-_{d_2}:=\mathbf{X}_{1d_2}$ and including the weighting factor

$$R^-_{d_2}(\xi^2):=\frac{w_{1d_2}B^2_{d_2}(\xi^2)}{\sum_{d_2=1}^{n_2}w_{1d_2}B^2_{d_2}(\xi^2)}. \tag{26}$$

Hence, only the knowledge of the knot vector Ξ^2 and a reduced set of control points together with the accompanying weights are sufficient to characterize the surface associated with ξ^1_-. The same

DOI: 10.1002/nme

principle applies for $\xi^1_+ = \xi^1_{n_1+p_1+1}$ and for the other dimension. Hence, in general, a univariate patch (in particular a contact patch) is directly inherited from the bivariate continuum patch and has its same parameterization but only with one parametric dimension that corresponds to any of the two dimensions. The corresponding knot vector is Ξ^α with associated B-spline basis functions $B^\alpha_{d_\alpha}$ and parametric space coordinate ξ^α that is conveniently chosen as the convective coordinate for contact computations. The surface parameterization is therefore

$$\mathbf{S}(\xi^2) = \sum_{d_2=1}^{n_2} R_{d_2}(\xi^2)\mathbf{X}_{d_2}. \tag{27}$$

Adopting the isoparametric concept, an analogous interpolation is used for the unknown displacement field, its variation and the current coordinates. For conciseness, these parameterizations will be expressed as follows:

$$\mathbf{S} = \sum_{A=1}^{n_{\mathrm{cp}}} R_A\mathbf{X}_A \quad \mathbf{u} = \sum_{A=1}^{n_{\mathrm{cp}}} R_A\mathbf{u}_A \quad \boldsymbol{\delta}\mathbf{u} = \sum_{A=1}^{n_{\mathrm{cp}}} R_A\boldsymbol{\delta}\mathbf{u}_A \quad \mathbf{x} = \sum_{A=1}^{n_{\mathrm{cp}}} R_A\mathbf{x}_A \tag{28}$$

where n_{cp} is the number of control points associated with the surface, R_A is the rational basis function corresponding to control point A, whereas $\mathbf{X}_A$, $\mathbf{u}_A$, $\delta\mathbf{u}_A$, and $\mathbf{x}_A$ are the related reference coordinate, displacement, displacement variation, and current coordinate vectors. Equation (28) can also be used for the Lagrange polynomial discretization, provided that the standard Lagrangian shape functions are used in place of R_A, and points A are interpreted as nodal points.

It is also useful to reconsider the above parameterization as a collection of local mappings, each defined over one individual element of the contact surface. The parameterization over an element e is

$$\mathbf{S}^e = \sum_{a=1}^{n_{\mathrm{nes}}} R_a\mathbf{X}_a \quad \mathbf{u}^e = \sum_{a=1}^{n_{\mathrm{nes}}} R_a\mathbf{u}_a \quad \boldsymbol{\delta}\mathbf{u}^e = \sum_{a=1}^{n_{\mathrm{nes}}} R_a\boldsymbol{\delta}\mathbf{u}_a \quad \mathbf{x}^e = \sum_{a=1}^{n_{\mathrm{nes}}} R_a\mathbf{x}_a \tag{29}$$

where $n_{\mathrm{nes}} = p_i + 1$ is the number of control points whose basis functions have support on a single element of the contact surface. Once again, Equation (29) can be also applied to a Lagrangian interpolation, in which case n_{nes} is simply the number of nodes per element of the contact surface. As follows, we will refer the above global and local parameterizations to the slave and the master surfaces by adding the appropriate superscript s or m, respectively.

4. VARIATIONS AND LINEARIZATIONS OF THE CONTACT VARIABLES IN DISCRETIZED FORM

By substituting the interpolations in Equation (29) into Equation (5a), the normal gap becomes

$$g_N = \left[\sum_{a=1}^{n^{\mathrm{s}}_{\mathrm{nes}}} R^{\mathrm{s}}_a(\xi^{\mathrm{s}})\mathbf{x}^{\mathrm{s}}_a - \sum_{a=1}^{n^{\mathrm{m}}_{\mathrm{nes}}} R^{\mathrm{m}}_a(\overline{\xi})\mathbf{x}^{\mathrm{m}}_a\right]\cdot\mathbf{n}. \tag{30}$$

In Equation (30), ξ^{s} is the parametric coordinate of the generic point on Γ_{c0}, whereas $\overline{\xi}$ is the parametric coordinate of the corresponding projection point on the master surface. The virtual variation follows from Equation (14a) as

$$\delta g_N = \left[\sum_{a=1}^{n^{\mathrm{s}}_{\mathrm{nes}}} R^{\mathrm{s}}_a(\xi^{\mathrm{s}})\boldsymbol{\delta}\mathbf{u}^{\mathrm{s}}_a - \sum_{a=1}^{n^{\mathrm{m}}_{\mathrm{nes}}} R^{\mathrm{m}}_a(\overline{\xi})\boldsymbol{\delta}\mathbf{u}^{\mathrm{m}}_a\right]\cdot\mathbf{n}. \tag{31}$$

By substituting the interpolations in Equation (29) into Equation (14c), the virtual variation $\delta\overline{\xi}$ becomes

$$\delta\overline{\xi} = \frac{1}{m_{11} - g_N k_{11}}\left[\left(\sum_{a=1}^{n^{\mathrm{s}}_{\mathrm{nes}}} R^{\mathrm{s}}_a(\xi^{\mathrm{s}})\boldsymbol{\delta}\mathbf{u}^{\mathrm{s}}_a - \sum_{a=1}^{n^{\mathrm{m}}_{\mathrm{nes}}} R^{\mathrm{m}}_a(\overline{\xi})\boldsymbol{\delta}\mathbf{u}^{\mathrm{m}}_a\right)\cdot\boldsymbol{\tau}_1 + g_N\mathbf{n}\cdot\sum_{a=1}^{n^{\mathrm{m}}_{\mathrm{nes}}} R^{\mathrm{m}}_{a,1}(\overline{\xi})\boldsymbol{\delta}\mathbf{u}^{\mathrm{m}}_a\right]. \tag{32}$$

DOI: 10.1002/nme

The same substitution can be carried out for the other equations in Section 2.4. Defining the vectors

$$\delta\mathbf{u}=\begin{bmatrix}\boldsymbol{\delta}\mathbf{u}_1^{\mathrm{s}}\\ \vdots\\ \boldsymbol{\delta}\mathbf{u}_{n_{\mathrm{nes}}^{\mathrm{s}}}^{\mathrm{s}}\\ \boldsymbol{\delta}\mathbf{u}_1^{\mathrm{m}}\\ \vdots\\ \boldsymbol{\delta}\mathbf{u}_{n_{\mathrm{nes}}^{\mathrm{m}}}^{\mathrm{m}}\end{bmatrix}\quad \Delta\mathbf{u}=\begin{bmatrix}\Delta\mathbf{u}_1^{\mathrm{s}}\\ \vdots\\ \Delta\mathbf{u}_{n_{\mathrm{nes}}^{\mathrm{s}}}^{\mathrm{s}}\\ \Delta\mathbf{u}_1^{\mathrm{m}}\\ \vdots\\ \Delta\mathbf{u}_{n_{\mathrm{nes}}^{\mathrm{m}}}^{\mathrm{m}}\end{bmatrix} \tag{33}$$

$$\mathbf{N}=\begin{bmatrix}R_1^{\mathrm{s}}(\xi^{\mathrm{s}})\mathbf{n}\\ \vdots\\ R_{n_{\mathrm{nes}}^{\mathrm{s}}}^{\mathrm{s}}(\xi^{\mathrm{s}})\mathbf{n}\\ -R_1^{\mathrm{m}}(\overline{\xi})\mathbf{n}\\ \vdots\\ -R_{n_{\mathrm{nes}}^{\mathrm{m}}}^{\mathrm{m}}(\overline{\xi})\mathbf{n}\end{bmatrix}\quad \mathbf{T}=\begin{bmatrix}R_1^{\mathrm{s}}(\xi^{\mathrm{s}})\boldsymbol{\tau}_1\\ \vdots\\ R_{n_{\mathrm{nes}}^{\mathrm{s}}}^{\mathrm{s}}(\xi^{\mathrm{s}})\boldsymbol{\tau}_1\\ -R_1^{\mathrm{m}}(\overline{\xi})\boldsymbol{\tau}_1\\ \vdots\\ -R_{n_{\mathrm{nes}}^{\mathrm{m}}}^{\mathrm{m}}(\overline{\xi})\boldsymbol{\tau}_1\end{bmatrix} \tag{34}$$

$$\mathbf{N}_1=\begin{bmatrix}\mathbf{0}\\ \vdots\\ \mathbf{0}\\ -R_{1,1}^{\mathrm{m}}(\overline{\xi})\mathbf{n}\\ \vdots\\ -R_{n_{\mathrm{nes}},1}^{\mathrm{m}}(\overline{\xi})\mathbf{n}\end{bmatrix}\quad \mathbf{T}_1=\begin{bmatrix}\mathbf{0}\\ \vdots\\ \mathbf{0}\\ -R_{1,1}^{\mathrm{m}}(\overline{\xi})\boldsymbol{\tau}_1\\ \vdots\\ -R_{n_{\mathrm{nes}},1}^{\mathrm{m}}(\overline{\xi})\boldsymbol{\tau}_1\end{bmatrix}\quad \mathbf{N}_{11}=\begin{bmatrix}\mathbf{0}\\ \vdots\\ \mathbf{0}\\ -R_{1,11}^{\mathrm{m}}(\overline{\xi})\mathbf{n}\\ \vdots\\ -R_{n_{\mathrm{nes}},11}^{\mathrm{m}}(\overline{\xi})\mathbf{n}\end{bmatrix} \tag{35}$$

$$\mathbf{D}_1=\frac{1}{m_{11}-k_{11}g_N}[\mathbf{T}-g_N\mathbf{N}_1]\quad \bar{\mathbf{N}}_1=\mathbf{N}_1-k_{11}\mathbf{D}_1\quad \bar{\mathbf{T}}_1=\mathbf{T}_1-\boldsymbol{\tau}_1\cdot\overline{\mathbf{x}}_{,\xi\xi}^{\mathrm{m}}\mathbf{D}_1 \tag{36}$$

Equations (31) and (32) (and the similar ones giving the linearized increments) can be cast in matrix form as

$$\delta g_N=\delta\mathbf{u}^{\mathrm{T}}\mathbf{N}\quad \delta\overline{\xi}=\delta\mathbf{u}^{\mathrm{T}}\mathbf{D}_1 \tag{37}$$

$$\Delta g_N=\mathbf{N}^{\mathrm{T}}\Delta\mathbf{u}\quad \Delta\overline{\xi}=\mathbf{D}_1^{\mathrm{T}}\Delta\mathbf{u} \tag{38}$$

moreover, Equations (15) and (16) become (in the form of the linearized increment)

$$\Delta t_{T_1}^{\mathrm{trial}}=\varepsilon_T[m_{11}\mathbf{D}_1^{\mathrm{T}}-2\overline{T}_1^{\mathrm{T}}(\overline{\xi}-\overline{\xi}_n)]\Delta\mathbf{u} \tag{39}$$

$$\Delta t_{T_1}=\mu\varepsilon_N\mathrm{sign}(t_{T_1}^{\mathrm{trial}})\left[\sqrt{m_{11}}\mathbf{N}^{\mathrm{T}}+\frac{g_N}{\sqrt{m_{11}}}\overline{\mathbf{T}}_1^{\mathrm{T}}\right]\Delta\mathbf{u} \tag{40}$$

for the stick and slip cases, respectively, and the linearizations $\Delta\delta g_N$ and $\Delta\delta\overline{\xi}$ can be expressed as

$$\Delta\delta g_N=\delta\mathbf{u}^{\mathrm{T}}\left[-\frac{g_N}{m_{11}}\bar{\mathbf{N}}_1\bar{\mathbf{N}}_1^{\mathrm{T}}-\mathbf{D}_1\mathbf{N}_1^{\mathrm{T}}-\mathbf{N}_1\mathbf{D}_1^{\mathrm{T}}+k_{11}\mathbf{D}_1\mathbf{D}_1^{\mathrm{T}}\right]\Delta\mathbf{u} \tag{41}$$

DOI: 10.1002/nme

$$\Delta\delta\overline{\xi} = \frac{1}{m_{11} - g_N k_{11}} \delta\mathbf{u}^{\mathrm{T}} \Big[2(\mathbf{T}_1\mathbf{D}_1^{\mathrm{T}} + \mathbf{D}_1\mathbf{T}_1^{\mathrm{T}}) - (3\boldsymbol{\tau}_1 \cdot \overline{\mathbf{x}}^{\mathrm{m}}_{,11} - g_N \mathbf{n} \cdot \overline{\mathbf{x}}^{\mathrm{m}}_{,111})\mathbf{D}_1\mathbf{D}_1^{\mathrm{T}} - g_N(\mathbf{N}_{11}\mathbf{D}_1^{\mathrm{T}} + \mathbf{D}_1\mathbf{N}_{11}^{\mathrm{T}}) - \mathbf{N}\overline{\mathbf{N}}_1^{\mathrm{T}} - \overline{\mathbf{N}}_1\mathbf{N}^{\mathrm{T}} - \frac{1}{m_{11}}(\mathbf{T}\overline{\mathbf{T}}_1^{\mathrm{T}} + \overline{\mathbf{T}}_1\mathbf{T}^{\mathrm{T}}) \Big] \Delta\mathbf{u}. \tag{42}$$

5. MORTAR-BASED CONTACT ALGORITHM

Two different contact algorithms are used in this work. The first (briefly referred to as 'non-mortar') consists in the enforcement of the contact constraints at each of the quadrature points associated with the contribution δW_{c}, as done in Fischer and Wriggers [21, 22]. Temizer *et al.* [15] already showed for NURBS discretizations that this approach delivers an excessively stiff contact constraint enforcement, which results in undesirable oscillations of the contact pressures when using large penalty parameters. The second algorithm is based on the mortar method [15, 23–28]. With this approach, the contact constraints are only enforced at the control points in the NURBS discretization, and at the nodes in the Lagrange discretization. Like in Tur *et al.* [27], integration is here carried out without segmentation of the contact surfaces to avoid the associated computational cost. For general discretizations this procedure will introduce an error, which can however be reduced by increasing the number of integration points on the contact surface, see also Fischer Wriggers [21].

The non-mortar approach implemented in this work is a straightforward extension to the NURBS discretization of the treatment presented by Fischer and Wriggers [21, 22]. For this reason, only the mortar algorithm is illustrated as follows. In the spirit of the mortar method, the contact contribution to the virtual work is expressed as

$$\delta W_{\mathrm{c}} = \sum_A (p_{NA}\delta g_{NA} + t_{TA}\delta\overline{\xi}_A) A_A \tag{43}$$

where the summation is extended to the active control points. The control point normal gap and parametric projections are defined as the weighted average of the corresponding 'local' quantities, with the basis functions as weights

$$g_{NA} = \frac{\int_{\Gamma_{\mathrm{c}0}} R_A g_N \,\mathrm{d}\Gamma}{\int_{\Gamma_{\mathrm{c}0}} R_A \,\mathrm{d}\Gamma} \quad \overline{\xi}_A = \frac{\int_{\Gamma_{\mathrm{c}0}} R_A \overline{\xi} \,\mathrm{d}\Gamma}{\int_{\Gamma_{\mathrm{c}0}} R_A \,\mathrm{d}\Gamma}. \tag{44}$$

An active control point is one for which $g_{NA} \leqslant 0$. With the above definition of the slip based on the parametric coordinate, care must be taken in the event that several NURB domains are merged to account for the change in the parametric coordinate at the junction. Alternative definitions are possible to avoid this necessity.

The virtual variation of Equation (44) gives

$$\delta g_{NA} = \frac{\int_{\Gamma_{\mathrm{c}0}} R_A \delta g_N \,\mathrm{d}\Gamma}{\int_{\Gamma_{\mathrm{c}0}} R_A \,\mathrm{d}\Gamma} \quad \delta\overline{\xi}_A = \frac{\int_{\Gamma_{\mathrm{c}0}} R_A \delta\overline{\xi} \,\mathrm{d}\Gamma}{\int_{\Gamma_{\mathrm{c}0}} R_A \,\mathrm{d}\Gamma}. \tag{45}$$

A control point value of the metric

$$m_{11A} = \frac{\int_{\Gamma_{\mathrm{c}0}} R_A m_{11} \,\mathrm{d}\Gamma}{\int_{\Gamma_{\mathrm{c}0}} R_A \,\mathrm{d}\Gamma} \tag{46}$$

is further introduced. Using the penalty method, the control point normal pressure is

$$p_{NA} = \varepsilon_N g_{NA}. \tag{47}$$

In the tangential direction, we can define a 'trial' control point tangential traction as

$$t_{TA}^{\mathrm{trial}} = t_{TA_n} + \varepsilon_T m_{11A}(\overline{\xi}_A - \overline{\xi}_{An}). \tag{48}$$

DOI: 10.1002/nme

The control point tangential traction will then be

$$t_{TA} = \begin{cases} t_{TA}^{\text{trial}} & \text{if } |t_{TA}^{\text{trial}}| \leqslant |\mu t_{NA}| \\ \mu |t_{NA}| \dfrac{t_{TA}^{\text{trial}}}{\|\mathbf{t}_{TA}^{\text{trial}}\|} = -\mu \varepsilon_N g_{NA} \dfrac{t_{TA}^{\text{trial}}}{\|\mathbf{t}_{TA}^{\text{trial}}\|} & \text{otherwise.} \end{cases} \tag{49}$$

Finally, the 'area of competence' of a control point is defined as

$$A_A = \int_{\Gamma_{c0}} R_A \, \mathrm{d}\Gamma. \tag{50}$$

Substituting the above definitions into Equation (43) yields

$$\begin{aligned} \delta W_c &= \sum_A \left(\varepsilon_N g_{NA} \int_{\Gamma_{c0}} R_A \delta g_N \, \mathrm{d}\Gamma + t_{TA} \int_{\Gamma_{c0}} R_A \delta \overline{\xi} \, \mathrm{d}\Gamma \right) \\ &= \int_{\Gamma_{c0}} \left[\varepsilon_N \left(\sum_A g_{NA} R_A \right) \delta g_N + \left(\sum_A t_{TA} R_A \right) \delta \overline{\xi} \right] \mathrm{d}\Gamma \\ &= \int_{\Gamma_{c0}} [p_{\text{Nint}} \delta g_N + t_{\text{Tint}} \delta \overline{\xi}] \, \mathrm{d}\Gamma \end{aligned} \tag{51}$$

where

$$p_{\text{Nint}} = \varepsilon_N \sum_A g_{NA} R_A \quad t_{\text{Tint}} = \sum_A t_{TA} R_A \tag{52}$$

are interpolated values of the contact normal pressure and tangential traction, respectively.

The combination of Equations (37) and (51) results in

$$\delta W_c = \delta \mathbf{u}^{\mathrm{T}} \int_{\Gamma_{c0}} [p_{\text{Nint}} \mathbf{N} + t_{\text{Tint}} \mathbf{D}_1] \, \mathrm{d}\Gamma. \tag{53}$$

From Equation (53) the expression of the residual for the Newton–Rapson iterative scheme is immediately obtained as

$$\mathbf{R} = \int_{\Gamma_{c0}} [p_{\text{Nint}} \mathbf{N} + t_{\text{Tint}} \mathbf{D}_1] \, \mathrm{d}\Gamma \tag{54}$$

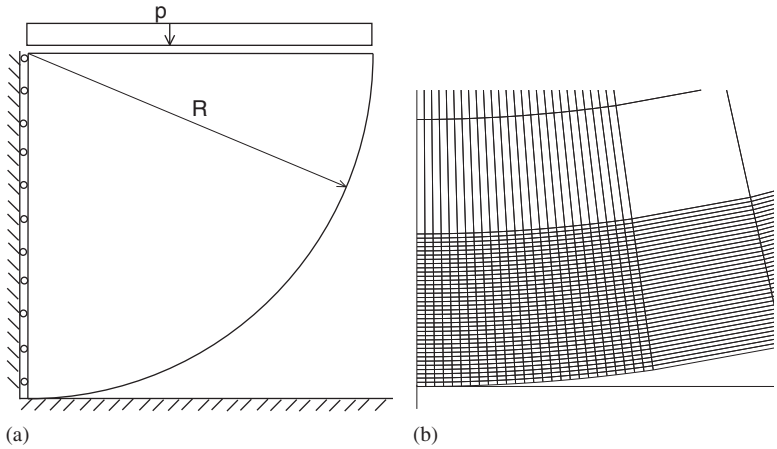

Figure 1. Example 1. (a) Problem scheme. $R = 1$, $p = 0.001$. (b) Close-up of the mesh (72×48) in the contact region.

DOI: 10.1002/nme

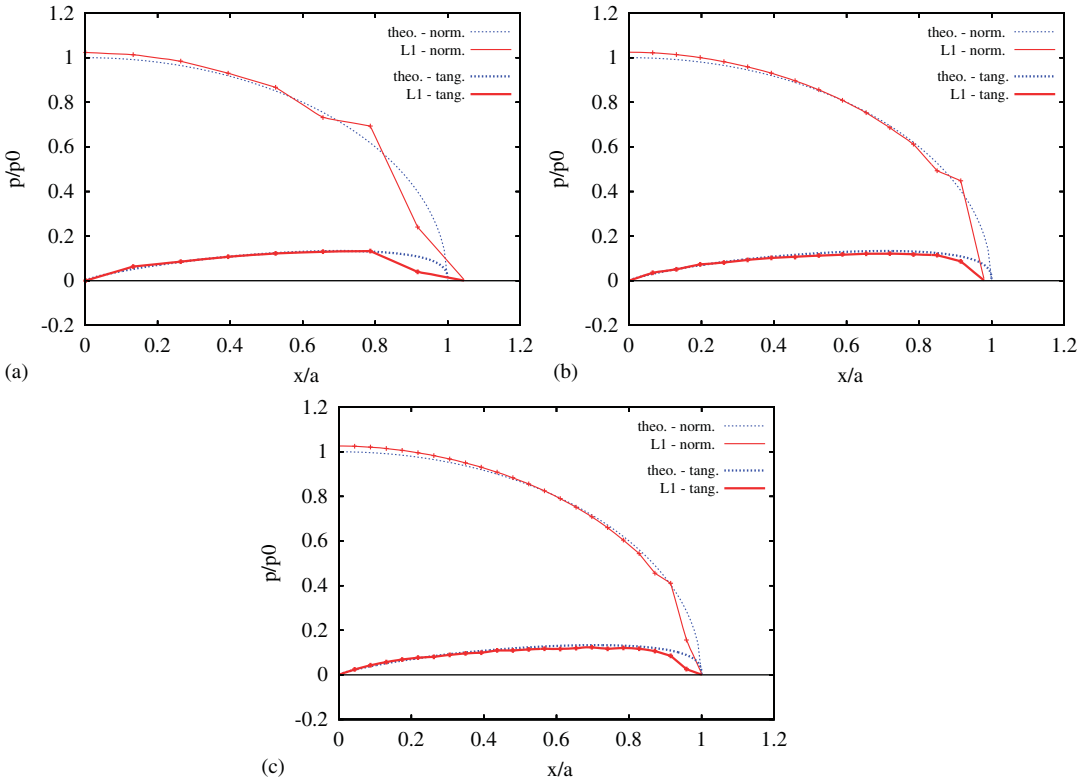

Figure 2. Effect of resolution for linear discretizations: (a) 36×24; (b) 72×48; and (c) 108×48.

As mentioned earlier, numerical integration is conducted directly on Γ_{c0} without segmentation of the contact surfaces, so that the residual in Equation (54) is numerically evaluated as follows:

$$\mathbf{R}=\sum_{GP}(p_{\mathrm{Nint}_g}\mathbf{N}_g+t_{\mathrm{Tint}_g}\mathbf{D}_{1g})w_g j_g \tag{55}$$

where the summation is extended to the Gauss points, subscript g refers to the dependence on the Gauss point coordinate, w_g and j_g are, respectively, the weight and the jacobian associated to the gth integration point on Γ_{c0}, and

$$p_{\mathrm{Nint}_g}=\varepsilon_N\sum_A g_{NA}R_{A_g}\quad t_{\mathrm{Tint}_g}=\sum_A t_{TA}R_{A_g}. \tag{56}$$

In Equation (56), R_{A_g} is the value at the gth integration point of the basis function associated with control point A. The full linearization and the consequent expression of the consistent tangent stiffness matrix are reported in the Appendix.

6. NUMERICAL EXAMPLES

This section presents three examples to demonstrate the accuracy and quality of the proposed contact formulation. For comparison purposes, not only NURBS but also Lagrange discretizations are employed. In the latter case, generation of the geometry and refinement are first conducted on the exact NURBS parameterization, and then converted to the Lagrange one.

The first two examples consider infinitesimal deformations in order to allow the comparison with available analytical solutions. The third example involves large deformations. In the first two examples, the mesh is refined in the vicinity of the contact region by redistributing the knot vector entries as already described in Temizer *et al.* [15]. The legends of the figures indicate the number of subdivisions used during h-refinement, i.e. the number of non-zero interior knot spans introduced

DOI: 10.1002/nme

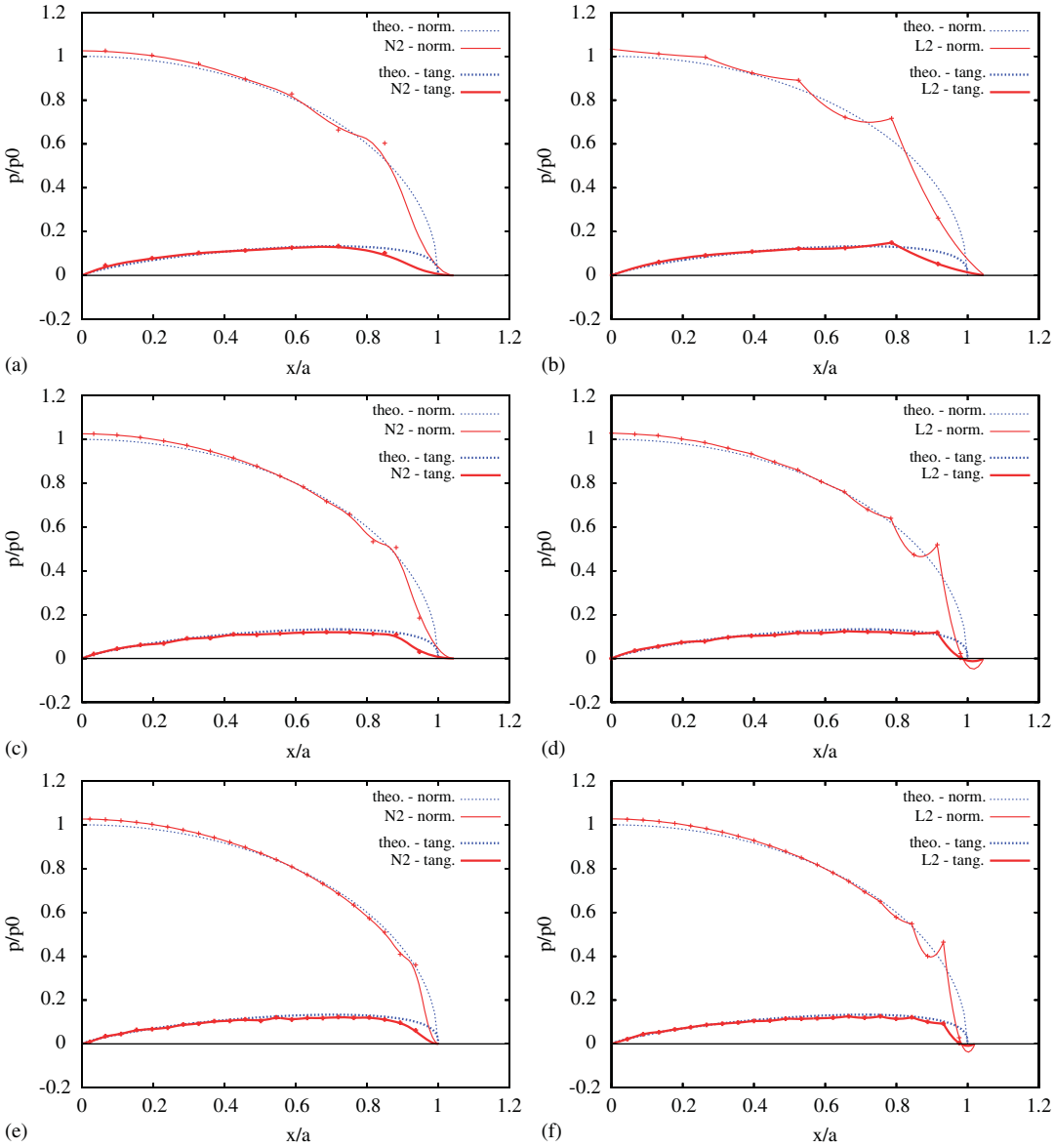

Figure 3. Effect of resolution for second-order NURBS and Lagrange discretizations: (a) 36×24; (b) 36×24; (c) 72×48; (d) 72×48; (e) 108×48; and (f) 108×48.

in the NURBS discretization in each parametric direction, e.g. 36×24. In the NURBS case, the number of subdivisions coincides with the number of elements in each direction. In the Lagrange parameterization, the number of elements in each direction is equal to the number of subdivisions divided by the order of the polynomial. Although the resulting number of control variables (control points or nodes) is different in the two cases, the resolution of the contact surface, as expressed by the number of contact facets, is the same and hence a direct comparison of the contact stresses is meaningful.

6.1. Hertz contact problem on rigid substrate

The first example deals with frictional contact of a cylinder of radius $R=1$ on a rigid plane. The material of the cylinder is linearly elastic with Young's modulus $E=1$ and Poisson's ratio $\nu=0.375$. Only a quarter of the geometry is considered, see Figure 1(a). The penalty parameters

DOI: 10.1002/nme

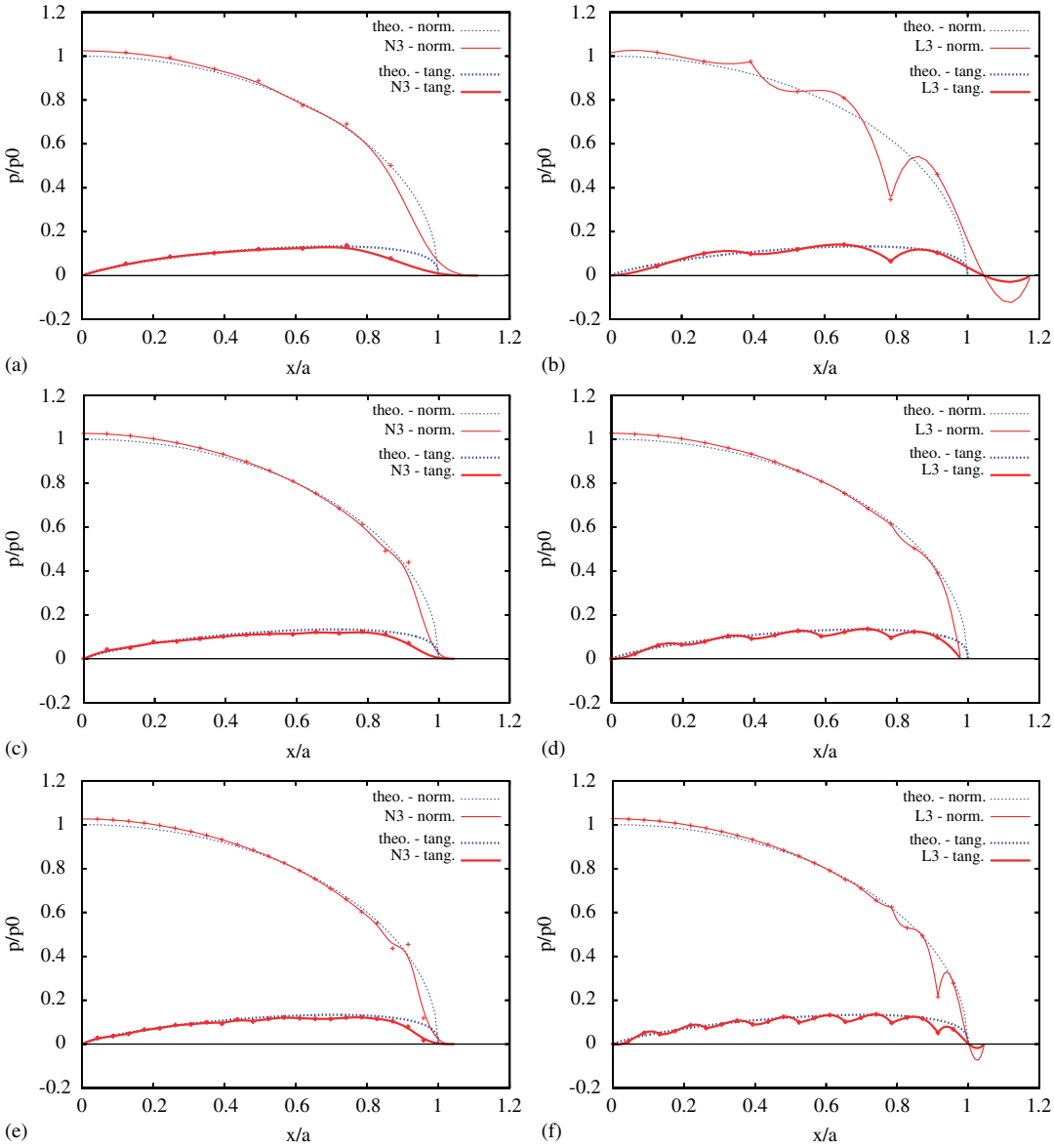

Figure 4. Effect of resolution for third-order NURBS and Lagrange discretizations: (a) 36×24; (b) 36×24; (c) 72×48; (d) 72×48; (e) 108×48; and (f) 108×48.

are $\varepsilon_N=10^4$ and $\varepsilon_T=10^3$, the friction coefficient is $\mu=0.8$. A large friction coefficient reduces the error related to the uncoupled approximation in the analytical solution, as explained later.

The cylinder is loaded with a vertical force $P=0.001$ applied as distributed load on the upper surface. Three different meshes are considered to evaluate the effect of mesh refinements. In all cases, the mesh is refined close to the contact region, see Figure 1(b). In all three meshes, the chosen amount of redistribution of the knot vector entries is such that 75% of the elements is located within 10% of the total length of the knot vector.

The analytical solution for this problem is not available in closed form. However, a simplified solution can be obtained by assuming that the normal and tangential contact stresses are uncoupled, which leads to a slight underestimation of the contact pressures [29, 30].

Figure 2 illustrates the results obtained from linear (Lagrange) interpolations. The dimensionless contact pressure p/p_0 is plotted versus the dimensionless coordinate x/a, p_0 and a being, respectively, the maximum normal pressure and the half-width of the contact area as predicted

DOI: 10.1002/nme

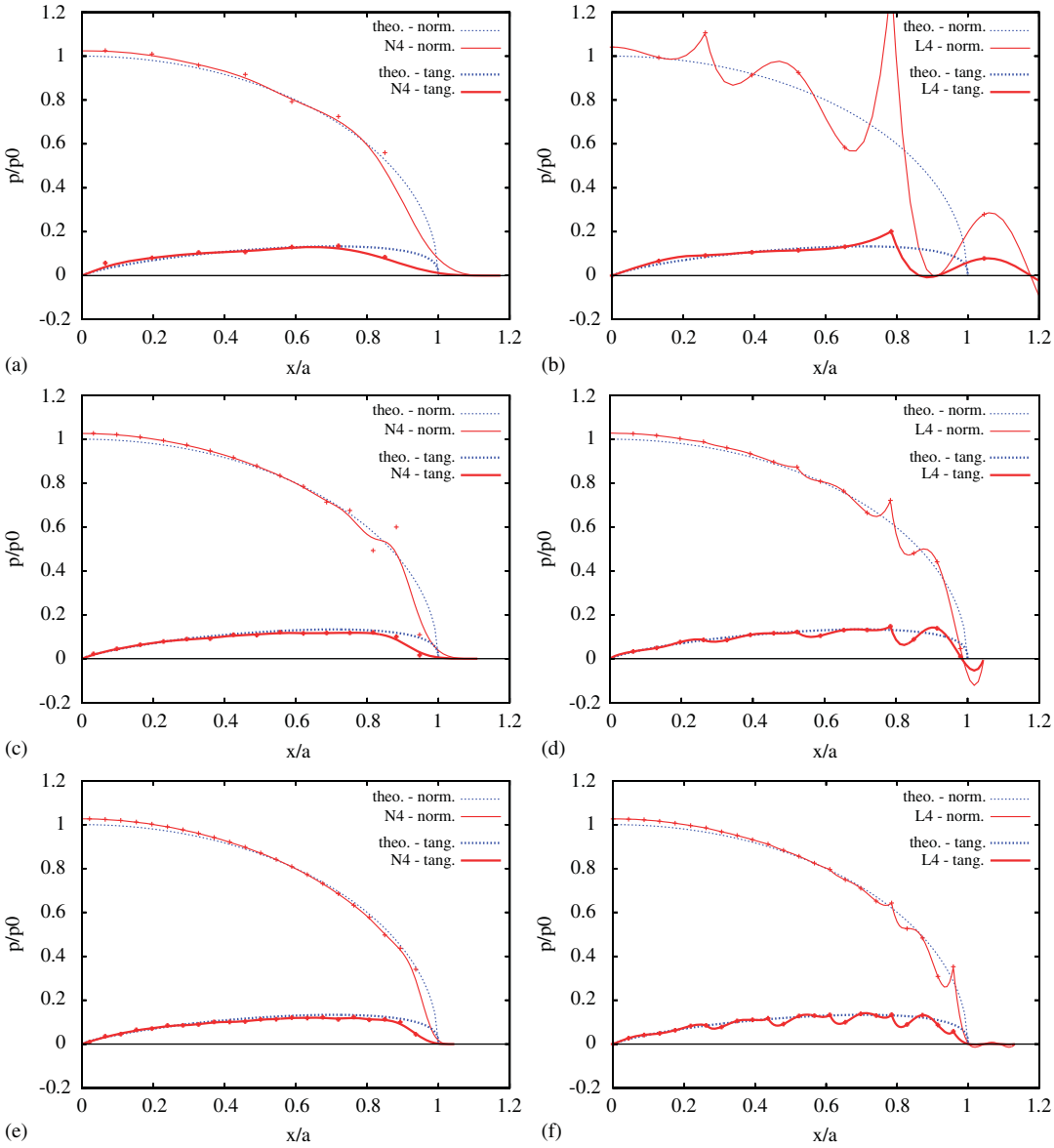

Figure 5. Effect of resolution for fourth-order NURBS and Lagrange discretizations: (a) 36×24; (b) 36×24; (c) 72×48; (d) 72×48; (e) 108×48; and (f) 108×48.

by the Hertz theory without friction. As already mentioned, the analytical solution is based on the uncoupling assumption, therefore a certain discrepancy with the numerical results is to be expected. Nevertheless, the agreement is generally very good. The solution near the edge of the contact region is affected by the elements that lie across the contact/non-contact zone. This is a well-known problem for which solutions have been proposed (see e.g. [31]). As the mesh is refined, the edge region is better resolved and the quality of the solution improves, as seen in Figure 2(c).

The results obtained with higher order NURBS and Lagrange discretizations are shown in Figures 3–5. The NURBS discretizations deliver a monotonic improvement of the pressure distribution quality with increasing resolution at a fixed order. For a given resolution, the quality of the results seems not to be affected by the order to an appreciable extent. Moreover, the oscillations of the contact pressure at the edge of the contact region are quite limited and all distributions feature non-negative values, due to the inherent non-negativeness of the NURBS basis functions. It

DOI: 10.1002/nme

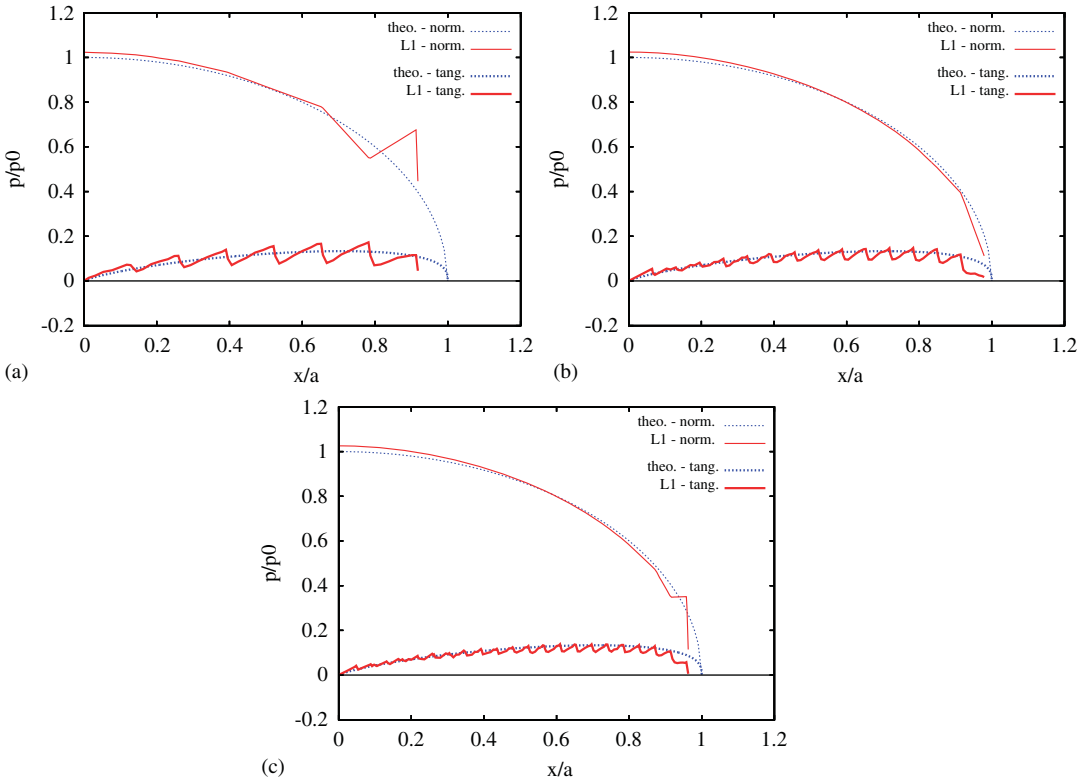

Figure 6. Effect of resolution for linear discretizations, using the non-mortar contact formulation: (a) 36×24; (b) 72×48; and (c) 108×48.

is evident that Lagrange discretizations produce results of inferior quality, especially as far as the frictional stresses are concerned. Also in this case the quality of the results tends to improve as the resolution is increased at a fixed order. However, even for the highest resolution, the distribution of the frictional stresses is highly irregular as a result of the C^0 continuity at the inter-element border, and possibly also of the negative values of the Lagrange shape functions. This problem of the C^0 continuity could be probably alleviated by introducing an averaging of the normal vectors at the interelement nodes such as done in Yang *et al.* [32], Puso and Laursen [24], Puso *et al.* [25]. This is obviously not needed for NURBS, as they guarantee the desired degree of continuity between adjacent contact elements. For a given resolution, increasing the order of the Lagrange discretization is evidently unfavorable, as even larger oscillations are produced. These oscillations, at the edge of the contact region, may result in high negative values which are not physically meaningful.

Finally, Figures 6 and 7 illustrate predictions of the 'non-mortar' approach for linear and second-order discretizations. Beside the fact that such predictions are highly sensitive to the value of the penalty parameter (as shown in Temizer *et al.* [15]), it is here evident that results of poor quality are obtained for the frictional stress distributions, with oscillations across the whole contact region whose size decreases with increased resolution. The mortar approach eliminates these oscillations through its non-local evaluation of the contact pressures. The same conclusion holds for both NURBS and Lagrange discretizations.

6.2. *Hertz contact problem between deformable bodies*

This example considers frictional contact between a deformable body having a cylindrical lower surface with radius of curvature $R = 1$ and a deformable plane (Figure 8(a)). The cylindrical surface is treated as slave, and the upper surface of the deformable plane as master. The mesh is refined close to the contact region, and the chosen amount of redistribution of the knot vector entries

DOI: 10.1002/nme

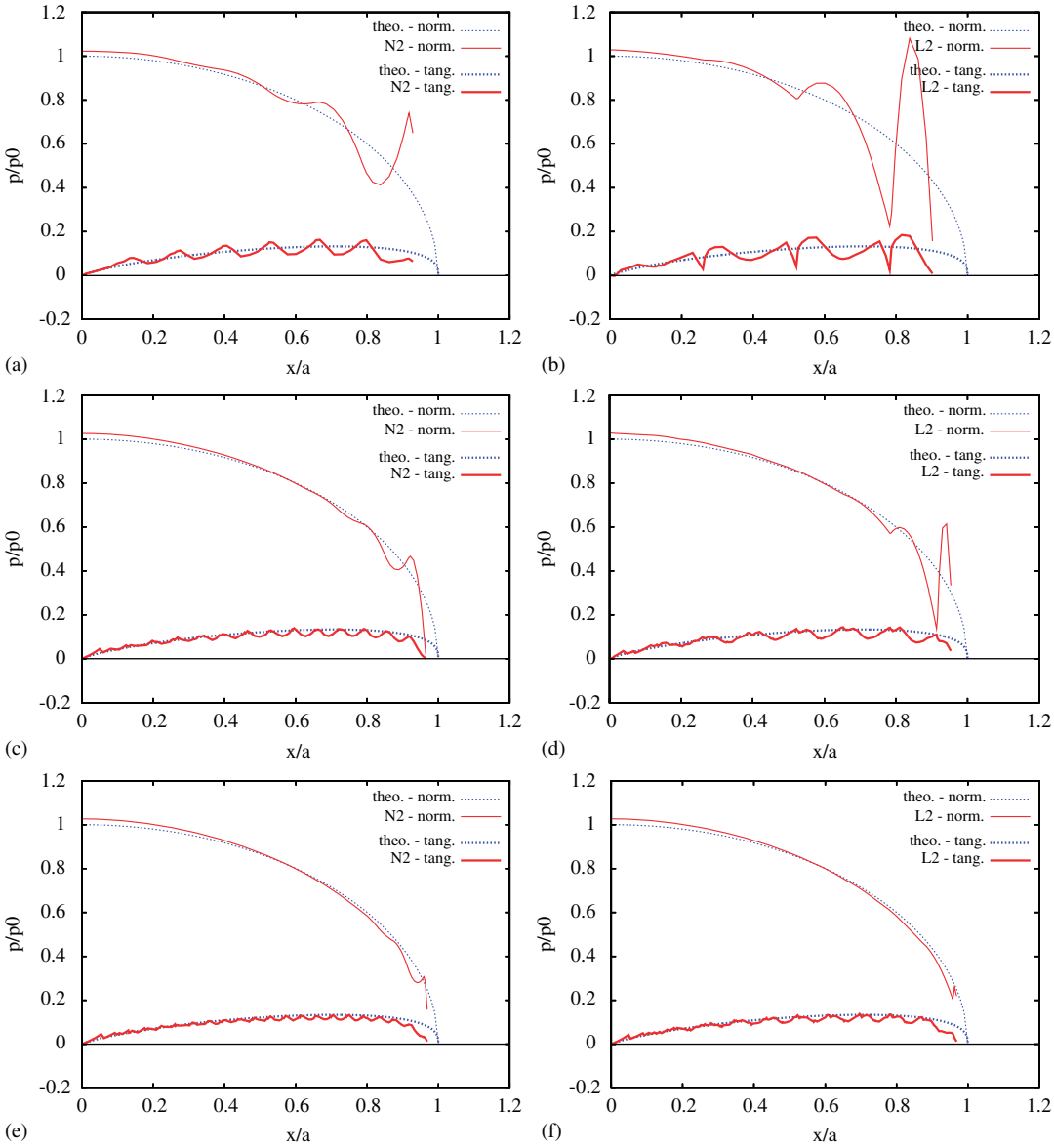

Figure 7. Effect of resolution for quadratic NURBS and Lagrange discretizations, using the non-mortar contact formulation: (a) 36×24; (b) 36×24; (c) 72×48; (d) 72×48; (e) 108×48; and (f) 108×48.

is such that 80% of the elements are located within 40% of the total length of the knot vector. Figure 8(b) shows the resulting configuration. The material of both bodies is linearly elastic with Young's modulus $E=1$ and Poisson's ratio $\nu=0.3$. The penalty parameters are $\varepsilon_N=10^4$ and $\varepsilon_T=10^3$, and the friction coefficient is $\mu=0.2$. The model is loaded with a vertical displacement, $v_{\max}=0.002$, and a horizontal displacement, $u_{\max}=0.00075$, both imposed on the upper surface. The corresponding total reaction forces on the upper surface are a normal force $P=0.0065$ and a tangential force $Q=0.001125$. The loading history is shown in Figure 9, while Figure 10 shows the final distribution of the σ_y stresses.

A closed-form analytical solution is available for this case [30], and is compared in Figure 11 with the results obtained from NURBS and Lagrange discretizations of different orders. The curves obtained from the NURBS interpolations are in excellent agreement with the analytical predictions. Once again, oscillations are present at the edge of the contact region, and could be eliminated by more finely resolving the contact/no contact interface. However, these oscillations are of limited

DOI: 10.1002/nme

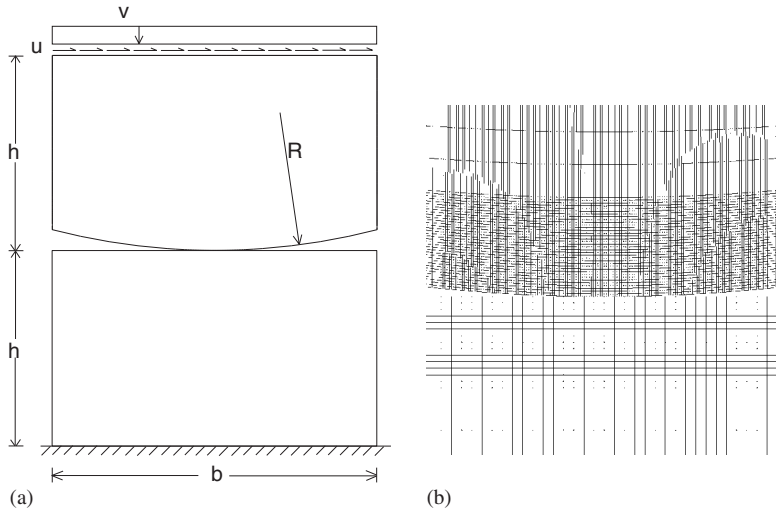

Figure 8. Example 2. (a) Problem scheme. $R=1$, $b=0.5$, $h=0.3$. (b) Close-up of the mesh in the contact region.

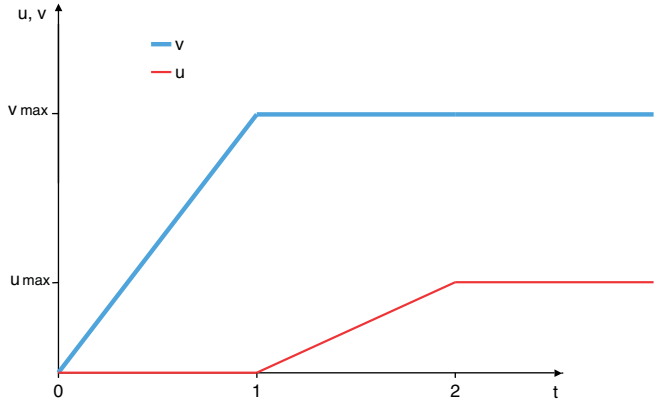

Figure 9. Loading history.

extent and only display non-negative values. Moreover, the quality of the solution is not affected by the order of the discretization. Conversely, the solution given by the Lagrange discretizations feature significant oscillations both at the edge of the contact region, where large negative values are at times predicted, and at the transitional zone between stick and slip conditions. Increasing the order appears in this case detrimental for the quality of the solution, due to the increasing incidence of spurious oscillations.

6.3. Ironing problem

In the third example, a cylindrical die is pressed into an elastic slab and then moved in the tangential direction. The lower surface of the die is treated as slave. Neo-Hookean hyper-elastic material behavior is assumed for both bodies, with material parameters $E=1$ and $\nu=0.3$ for the slab, and $E=1000$ and $\nu=0.3$ for the die. The geometric model is depicted in Figure 12(a). For this problem the penalty parameters are $\varepsilon_N=\varepsilon_T=10^2$, whereas the coefficient of friction is $\mu=0.3$. A uniform downward displacement $U_y=-0.075$ is applied to the upper line of the die in 10 time steps and then maintained constant while a horizontal displacement $U_x=2.0$ is applied in a further 140 time steps. The problem is solved using NURBS discretizations for both die and block, as well as Lagrange discretizations for comparison purposes. Figures 12(b)–(d) show the deformed mesh in the N2 case at different time steps.

DOI: 10.1002/nme

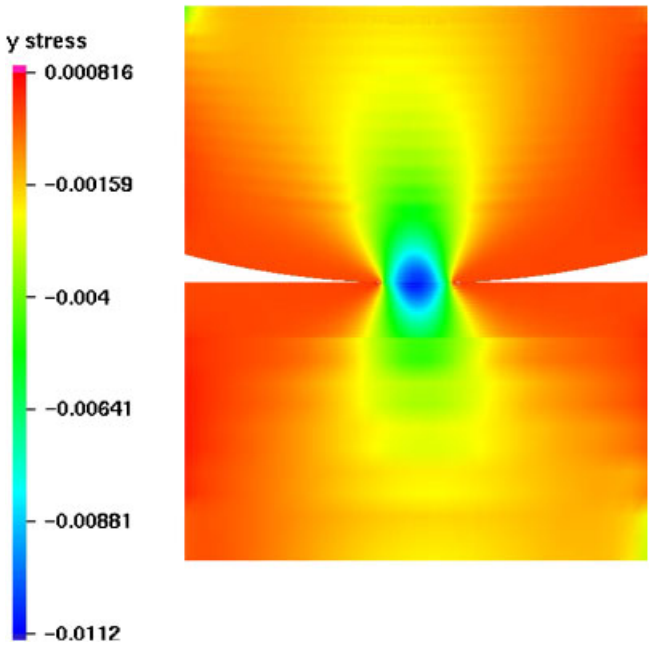

Figure 10. Distribution of stresses σ_y at the end of the loading history.

Figure 13(a) shows a plot of the total reaction forces in the horizontal and vertical directions, computed on the top line of the die as a function of time. Four sets of results are plotted, corresponding to linear and quadratic Lagrange discretizations, and to second- and fourth-order NURBS. Lagrange discretizations with orders higher than 2 yield no convergence for the above number of time steps. The N3 case was calculated but not plotted, its results being quite similar to those of the N2 case. For the sake of clarity, Figure 13(b) replots only the N4 results, and clearly shows the remarkable smoothness of both the normal and tangential force curves. The difference between the analyzed discretizations is visible in the close-ups of Figures 13(c) and (d) for the horizontal and vertical reaction force, respectively. At this close view the force oscillations due to the discretization are clearly visible. Similar oscillations for the ironing problem treated with both node-to-segment and mortar approaches have already been reported in the literature, see e.g. [24]. The parameterization exerts a clear influence on the magnitude and regularity of these oscillations. Both the linear and the quadratic Lagrange cases yield quite large and irregular force variations, with the second-order case giving the worst results. The lack of convergence for orders higher than 2 is probably due to a further increase in the magnitude of the oscillations, which worsens the iterative convergence performance. Using the second-order NURBS parameterization greatly improves the quality of results, as visible from the reduced magnitude of the oscillations and from their more regular pattern. This result stems from the higher degree of smoothness which is achieved through the higher inter-element continuity in the parameterization of both the bulk and the contact surface. Unlike for Lagrange discretizations, the results monotonically improve as the order of the NURBS discretization increases. For instance, passing from N2 to N4 the magnitude of the oscillations is further reduced, and the resulting curves are already macroscopically smooth as seen in Figure 13(b). These observations thus extend the general results previously found in the small deformation examples to the case of large deformations and large frictional sliding.

7. CONCLUSIONS

This work focused on the performance of NURBS-based isogeometric analysis applied to large deformation Coulomb frictional contact problems, in particular as compared to standard

DOI: 10.1002/nme

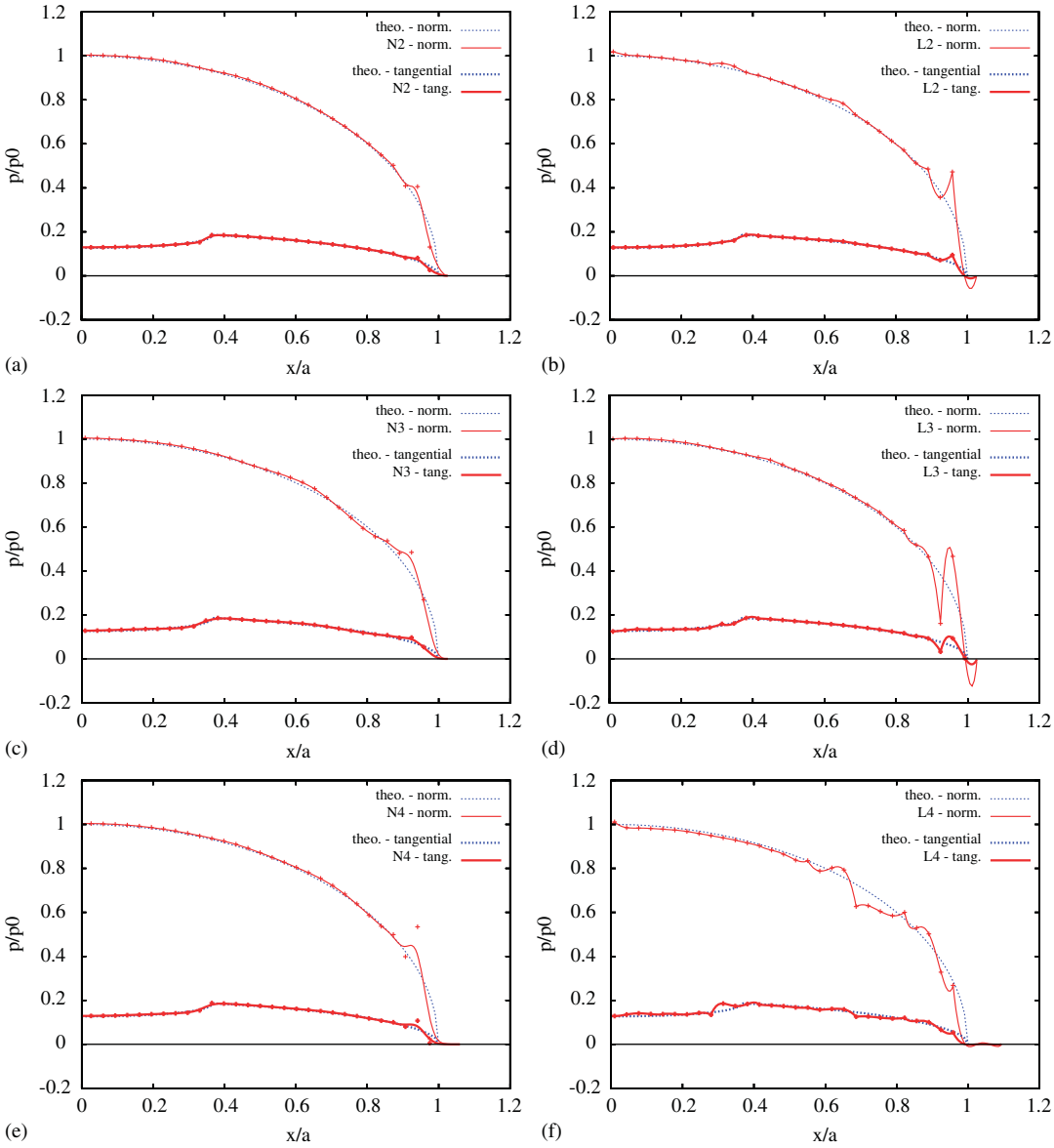

Figure 11. Effect of order for NURBS and Lagrange discretizations: (a) N2; (b) L2; (c) N3; (d) L3; (e) N4; and (f) L4.

C^0-continuous Lagrange finite element interpolations. Unlike in earlier works dealing with NURBS surface smoothing techniques, in this work the contact patches are inherited directly from the NURBS continuum parameterization. The proposed contact formulation is based on a mortar approach, extended to NURBS-based interpolations for both normal and frictional contact, and combined with a simple integration scheme which does not involve segmentation of the contact surfaces.

Based on the results obtained in this investigation, it can be concluded that the proposed frictional contact mortar formulation using NURBS-based isogeometric analysis displays a significantly superior performance with respect to the same formulation using standard Lagrange polynomials. The contact pressure distributions stemming from the NURBS parameterizations are always non-negative, are practically insensitive to changes in the interpolation order, and improve monotonically as the mesh resolution increases. The respective distributions obtained from Lagrange parameterizations are highly sensitive to the interpolation order, display significant spurious oscillations

DOI: 10.1002/nme

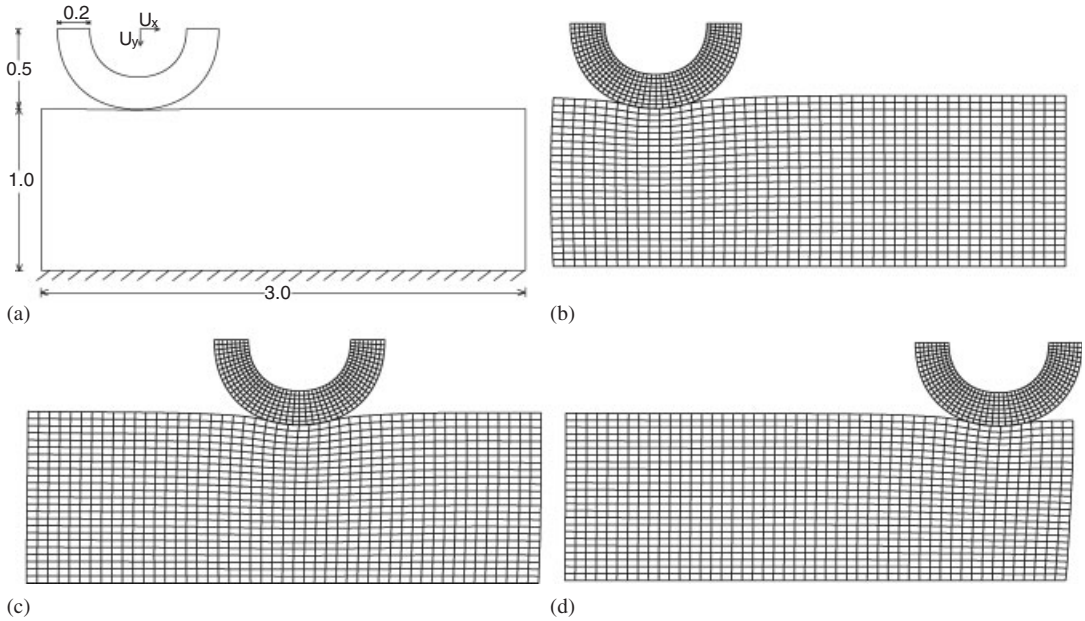

Figure 12. Example 3. (a) Problem scheme; (b) deformed mesh at time $t = 10$; (c) deformed mesh at time $t = 80$; and (d) deformed mesh at time $t = 150$.

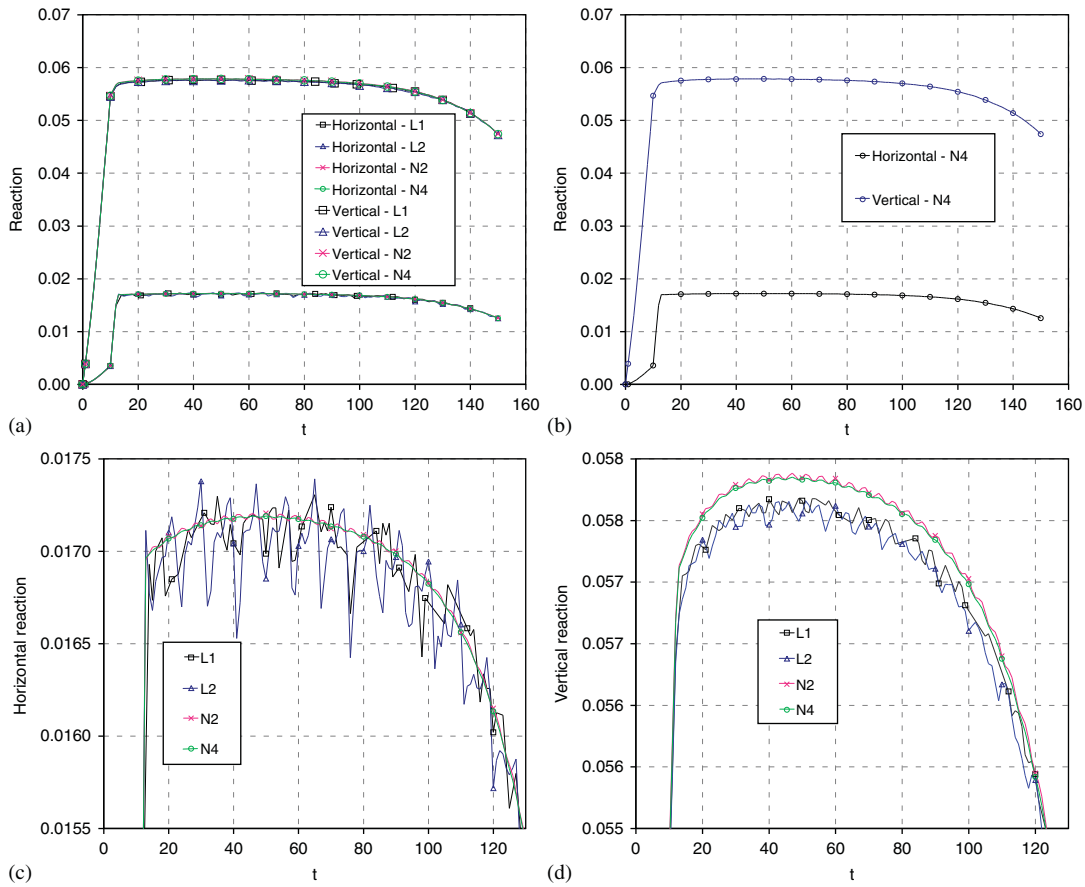

Figure 13. Reaction forces. (a) Horizontal and vertical reaction forces—all discretizations; (b) horizontal and vertical reaction forces—N4; (c) close-up of the horizontal reaction forces; and (d) close-up of the vertical reaction forces.

DOI: 10.1002/nme

and may attain large non-physical negative values. In large frictional sliding problems the time histories of the tractions obtained from the NURBS discretizations are remarkably smooth and improve in quality with increasing order of the parameterization. Conversely, the curves obtained from Lagrange parameterizations display irregular oscillations whose magnitude increases with the interpolation order and which may even prevent convergence.

This superiority of the NURBS parameterization over the Lagrange one for contact modeling is a combined effect of the higher continuity achieved at the inter-element boundaries and of the inherent non-negativeness of the NURBS interpolation functions. While these two favorable features may also be individually obtained in different ways (e.g. higher geometric continuity can be pursued by means of smoothing techniques and inherent non-negativeness is possessed by other categories of shape functions), NURBS-based isogeometric analysis provides a very simple framework in which both are simultaneously and naturally achieved. The individual role played by these two factors could be isolated e.g. by using C^0 Berstein polynomials, which are non-negative and possess the variation diminishing and convex hull properties like the NURBS basis. This is left as a potential topic for further investigations.

It was also shown that the non-mortar contact formulation delivers results of poor quality especially as far as the frictional stresses are concerned, due to the enforcement of the contact constraints at each integration point which leads to an over-constrained problem. Conversely, the mortar formulation eliminates this drawback by enforcing the contact constraints only at the control points (or nodal points for Lagrange interpolations).

The extension of the developed frictional contact formulation to the 3D setting and to the employment of alternative contact algorithms is currently underway.

APPENDIX A

The linearization of Equation (43) yields

$$\Delta\delta W_{\mathrm{c}} = \Delta\delta W_{\mathrm{c,m}} + \Delta\delta W_{\mathrm{c,g}} \tag{A1}$$

where

$$\begin{aligned}\Delta\delta W_{\mathrm{c,m}} &= \sum_A (\Delta p_{NA}\delta g_{NA} + \Delta t_{TA}\delta\bar{\xi}_A)A_A \\ &= \sum_A \varepsilon_N \Delta g_{NA}\delta g_{NA}A_A + \sum_{A,st} \Delta t_{TA}^{\mathrm{trial}}\delta\bar{\xi}_A A_A + \sum_{A,sl} \Delta t_{TA}\delta\bar{\xi}_A A_A\end{aligned} \tag{A2}$$

is the 'main' component, and

$$\begin{aligned}\Delta\delta W_{\mathrm{c,g}} &= \sum_A (p_{NA}\Delta\delta g_{NA} + t_{TA}\Delta\delta\bar{\xi}_A)A_A \\ &= \sum_A (\varepsilon_N g_{NA}\Delta\delta g_{NA} + t_{TA}\Delta\delta\bar{\xi}_A)A_A\end{aligned} \tag{A3}$$

is the 'geometric' component. In the frictional contribution to the main component, the summation must be conducted separately for the active control points in stick and for those in slip conditions.

By combining Equations (45) and (50) with Equation (A2), the main component $\Delta\delta W_{\mathrm{c,m}}$ can be expressed as

$$\begin{aligned}\Delta\delta W_{\mathrm{c,m}} = \sum_A &\left(\frac{\varepsilon_N}{\int_{\Gamma_{\mathrm{c0}}} R_A\,\mathrm{d}\Gamma}\int_{\Gamma_{\mathrm{c0}}} R_A\delta g_N\,\mathrm{d}\Gamma\int_{\Gamma_{\mathrm{c0}}} R_A\Delta g_N\,\mathrm{d}\Gamma\right) \\ &+ \sum_{A,st}\Delta t_{TA}^{\mathrm{trial}}\int_{\Gamma_{\mathrm{c0}}} R_A\delta\bar{\xi}\,\mathrm{d}\Gamma + \sum_{A,sl}\Delta t_{TA}\int_{\Gamma_{\mathrm{c0}}} R_A\delta\bar{\xi}\,\mathrm{d}\Gamma\end{aligned} \tag{A4}$$

DOI: 10.1002/nme

where, from Equations (48) and (49),

$$\Delta t_{TA}^{\text{trial}} = \varepsilon_T[\Delta m_{11A}(\overline{\xi}_A - \overline{\xi}_{An}) + m_{11A}\Delta\overline{\xi}_A] \tag{A5}$$

$$\Delta t_{TA} = -\mu\varepsilon_N \text{sign}(t_{TA}^{\text{trial}})\left[\sqrt{m_{11A}}\Delta g_{NA} + \frac{g_{NA}}{2\sqrt{m_{11A}}}\Delta m_{11A}\right] \tag{A6}$$

and, from the definition in Equation (46),

$$\Delta m_{11A} = \frac{\int_{\Gamma_{c0}} R_A \Delta m_{11}\,\mathrm{d}\Gamma}{\int_{\Gamma_{c0}} R_A\,\mathrm{d}\Gamma}. \tag{A7}$$

Substitution of Equations (A5) to (A7) into Equation (A4) and employment of the matrix expressions in Section 4 yields

$$\begin{aligned}
&\Delta\delta W_{\text{c,m}} \\
&= \delta\mathbf{u}^{\text{T}}\left\{\sum_A\left[\frac{\varepsilon_N}{\int_{\Gamma_{c0}} R_A\,\mathrm{d}\Gamma}\int_{\Gamma_{c0}} R_A\mathbf{N}\,\mathrm{d}\Gamma\int_{\Gamma_{c0}} R_A\mathbf{N}^{\text{T}}\,\mathrm{d}\Gamma\right]\right. \\
&+ \sum_{A,st}\left[\frac{\varepsilon_T}{\int_{\Gamma_{c0}} R_A\,\mathrm{d}\Gamma}\int_{\Gamma_{c0}} R_A\mathbf{D}_1\,\mathrm{d}\Gamma\int_{\Gamma_{c0}} R_A(m_{11A}\mathbf{D}_1^{\text{T}} - 2\overline{\mathbf{T}}_1^{\text{T}}(\overline{\xi}_A - \overline{\xi}_{An}))\,\mathrm{d}\Gamma\right] \\
&\left.+ \sum_{A,sl}\left[\frac{\mu\varepsilon_N \text{sign}(p_{TA,\text{trial}})}{\int_{\Gamma_{c0}} R_A\,\mathrm{d}\Gamma}\int_{\Gamma_{c0}} R_A\mathbf{D}_1\,\mathrm{d}\Gamma\int_{\Gamma_{c0}} R_A\left(\sqrt{m_{11A}}\mathbf{N}^{\text{T}} + \frac{g_{NA}}{\sqrt{m_{11A}}}\overline{\mathbf{T}}_1^{\text{T}}\right)\mathrm{d}\Gamma\right]\right\}\Delta\mathbf{u}.
\end{aligned} \tag{A8}$$

The geometric component in Equation (A3) can be rewritten as

$$\begin{aligned}
\Delta\delta W_{\text{c,g}} &= \sum_A\left(\varepsilon_N g_{NA}\int_{\Gamma_{c0}} R_A\Delta\delta g_N\,\mathrm{d}\Gamma + t_{TA}\int_{\Gamma_{c0}} R_A\Delta\delta\overline{\xi}\,\mathrm{d}\Gamma\right) \\
&= \int_{\Gamma_{c0}}\left[\varepsilon_N\left(\sum_A g_{NA}R_A\right)\Delta\delta g_N + \left(\sum_A t_{TA}R_A\right)\Delta\delta\overline{\xi}\right]\mathrm{d}\Gamma \\
&= \int_{\Gamma_{c0}}[p_{\text{Nint}}\Delta\delta g_N + t_{\text{Tint}}\Delta\delta\overline{\xi}]\,\mathrm{d}\Gamma
\end{aligned} \tag{A9}$$

where the linearization of Equation (45)

$$\Delta\delta g_{NA} = \frac{\int_{\Gamma_{c0}} R_A\Delta\delta g_N\,\mathrm{d}\Gamma}{\int_{\Gamma_{c0}} R_A\,\mathrm{d}\Gamma} \quad \Delta\delta\overline{\xi}_A = \frac{\int_{\Gamma_{c0}} R_A\Delta\delta\overline{\xi}\,\mathrm{d}\Gamma}{\int_{\Gamma_{c0}} R_A\,\mathrm{d}\Gamma} \tag{A10}$$

and Equations (50) and (52) have been employed. Combining Equation (A9) with the matrix expressions of $\Delta\delta g_N$ and $\Delta\delta\overline{\xi}$ in Equations (41) and (42) yields

$$\begin{aligned}
\Delta\delta W_{\text{c,g}} = \delta\mathbf{u}^{\text{T}}\int_{\Gamma_{c0}}\left\{\varepsilon_N p_{\text{Nint}}\left(-\frac{g_N}{m_{11}}\bar{\mathbf{N}}_1\bar{\mathbf{N}}_1^{\text{T}} - \mathbf{D}_1\mathbf{N}_1^{\text{T}} - \mathbf{N}_1\mathbf{D}_1^{\text{T}} + k_{11}\mathbf{D}_1\mathbf{D}_1^{\text{T}}\right)\right. \\
+ \frac{t_{\text{Tint}}}{m_{11} - g_N k_{11}}\left[2(\mathbf{T}_1\mathbf{D}_1^{\text{T}} + \mathbf{D}_1\mathbf{T}_1^{\text{T}}) - (3\boldsymbol{\tau}_1\cdot\overline{\mathbf{x}}_{,11}^{\text{m}} - g_N\mathbf{n}\cdot\overline{\mathbf{x}}_{,111}^{\text{m}})\cdot\mathbf{D}_1\mathbf{D}_1^{\text{T}}\right. \\
\left.\left. - g_N(\mathbf{N}_{11}\mathbf{D}_1^{\text{T}} + \mathbf{D}_1\mathbf{N}_{11}^{\text{T}}) - \mathbf{N}\overline{\mathbf{N}}_1^{\text{T}} - \overline{\mathbf{N}}_1\mathbf{N}^{\text{T}} - \frac{1}{m_{11}}(\mathbf{T}\overline{\mathbf{T}}_1^{\text{T}} + \overline{\mathbf{T}}_1\mathbf{T}^{\text{T}})\right]\right\}\mathrm{d}\Gamma\Delta\mathbf{u}.
\end{aligned} \tag{A11}$$

DOI: 10.1002/nme

Finally, the main and geometric components of the stiffness matrix, $\mathbf{K}_m$ and $\mathbf{K}_g$, are readily obtained from Equations (A8) and (A11) as

$$\begin{aligned}\mathbf{K}_{\mathrm{m}} &= \sum_A \left[\frac{\varepsilon_N}{\int_{\Gamma_{\mathrm{c}0}} R_A \,\mathrm{d}\Gamma} \int_{\Gamma_{\mathrm{c}0}} R_A \mathbf{N} \,\mathrm{d}\Gamma \int_{\Gamma_{\mathrm{c}0}} R_A \mathbf{N}^{\mathrm{T}} \,\mathrm{d}\Gamma \right] \\ &\quad + \sum_{A,st} \left[\frac{\varepsilon_T}{\int_{\Gamma_0} R_A \,\mathrm{d}\Gamma} \int_{\Gamma_{\mathrm{c}0}} R_A \mathbf{D}_1 \,\mathrm{d}\Gamma \int_{\Gamma_{\mathrm{c}0}} R_A (m_{11A} \mathbf{D}_1^{\mathrm{T}} - 2\overline{\mathbf{T}}_1^{\mathrm{T}} (\overline{\xi}_A - \overline{\xi}_{An})) \,\mathrm{d}\Gamma \right] \\ &\quad + \sum_{A,sl} \left[\frac{\mu \varepsilon_N \mathrm{sign}(p_{TA,\mathrm{trial}})}{\int_{\Gamma_0} R_A \,\mathrm{d}\Gamma} \int_{\Gamma_{\mathrm{c}0}} R_A \mathbf{D}_1 \,\mathrm{d}\Gamma \int_{\Gamma_{\mathrm{c}0}} R_A \left(\sqrt{m_{11A}} \mathbf{N}^{\mathrm{T}} + \frac{g_{NA}}{\sqrt{m_{11A}}} \overline{\mathbf{T}}_1^{\mathrm{T}} \right) \mathrm{d}\Gamma \right] \end{aligned} \tag{A12}$$

$$\begin{aligned}\mathbf{K}_{\mathrm{g}} &= \int_{\Gamma_{\mathrm{c}0}} \left\{ \varepsilon_N p_{\mathrm{Nint}} \left(-\frac{g_N}{m_{11}} \tilde{\mathbf{N}}_1 \tilde{\mathbf{N}}_1^{\mathrm{T}} - \mathbf{D}_1 \mathbf{N}_1^{\mathrm{T}} - \mathbf{N}_1 \mathbf{D}_1^{\mathrm{T}} + k_{11} \mathbf{D}_1 \mathbf{D}_1^{\mathrm{T}} \right) \right. \\ &\quad + \frac{t_{\mathrm{Tint}}}{m_{11} - g_N k_{11}} [2(\mathbf{T}_1 \mathbf{D}_1^{\mathrm{T}} + \mathbf{D}_1 \mathbf{T}_1^{\mathrm{T}}) - (3\boldsymbol{\tau}_1 \cdot \overline{\mathbf{x}}_{,11}^{\mathrm{m}} - g_N \mathbf{n} \cdot \overline{\mathbf{x}}_{,111}^{\mathrm{m}}) \\ &\quad \left. \times \mathbf{D}_1 \mathbf{D}_1^{\mathrm{T}} - g_N (\mathbf{N}_{11} \mathbf{D}_1^{\mathrm{T}} + \mathbf{D}_1 \mathbf{N}_{11}^{\mathrm{T}}) - \mathbf{N} \overline{\mathbf{N}}_1^{\mathrm{T}} - \overline{\mathbf{N}}_1 \mathbf{N}^{\mathrm{T}} - \frac{1}{m_{11}} (\mathbf{T} \overline{\mathbf{T}}_1^{\mathrm{T}} + \overline{\mathbf{T}}_1 \mathbf{T}^{\mathrm{T}}) \right] \right\} \mathrm{d}\Gamma \end{aligned} \tag{A13}$$

and the tangent stiffness matrix is simply

$$\mathbf{K} = \mathbf{K}_{\mathrm{m}} + \mathbf{K}_{\mathrm{g}}. \tag{A14}$$

The integrals in Equations (A12) and (A13) are carried out numerically as follows:

$$\begin{aligned}\mathbf{K}_{\mathrm{m}} &= \sum_A \left[\frac{\varepsilon_N}{\sum_{GP} R_{A_g} w_g j_g} \sum_{GP} R_{A_g} \mathbf{N}_{\mathrm{g}} w_g j_g \sum_{GP} R_{A_g} \mathbf{N}_g^{\mathrm{T}} w_g j_g \right] \\ &\quad + \sum_{A,st} \left[\frac{\varepsilon_T}{\sum_{GP} R_{A_g} w_g j_g} \sum_{GP} R_{A_g} \mathbf{D}_{1g} w_g j_g \sum_{GP} R_{A_g} (m_{11A} \mathbf{D}_{1g}^{\mathrm{T}} - 2\overline{\mathbf{T}}_{1g}^{\mathrm{T}} (\overline{\xi}_A - \overline{\xi}_{An})) w_g j_g \right] \\ &\quad + \sum_{A,sl} \left[\frac{\mu \varepsilon_N \mathrm{sign}(p_{TA,\mathrm{trial}})}{\sum_{GP} R_{A_g} w_g j_g} \sum_{GP} R_{A_g} \mathbf{D}_{1g} w_g j_g \sum_{GP} R_{A_g} \left(\sqrt{m_{11A}} \mathbf{N}_g^{\mathrm{T}} + \frac{g_{NA}}{\sqrt{m_{11A}}} \overline{\mathbf{T}}_{1g}^{\mathrm{T}} \right) w_g j_g \right] \end{aligned} \tag{A15}$$

$$\begin{aligned}\mathbf{K}_{\mathrm{g}} &= \sum_{GP} \left\{ \varepsilon_N p_{\mathrm{Nint}_g} \left(-\frac{g_{N_g}}{m_{11_g}} \tilde{\mathbf{N}}_{1g} \tilde{\mathbf{N}}_{1g}^{\mathrm{T}} - \mathbf{D}_{1g} \mathbf{N}_{1g}^{\mathrm{T}} - \mathbf{N}_{1g} \mathbf{D}_{1g}^{\mathrm{T}} + k_{11g} \mathbf{D}_{1g} \mathbf{D}_{1g}^{\mathrm{T}} \right) \right. \\ &\quad + \frac{t_{\mathrm{Tint}_g}}{m_{11_g} - g_{N_g} k_{11_g}} \left[2(\mathbf{T}_{1g} \mathbf{D}_{1g}^{\mathrm{T}} + \mathbf{D}_{1g} \mathbf{T}_{1g}^{\mathrm{T}}) - (3\boldsymbol{\tau}_{1g} \cdot \overline{\mathbf{x}}_{,11g}^{\mathrm{m}} - g_{Ng} \mathbf{n}_g \cdot \overline{\mathbf{x}}_{,111g}^{\mathrm{m}}) \right. \\ &\quad \left. \left. \times \mathbf{D}_{1g} \mathbf{D}_{1g}^{\mathrm{T}} - g_{Ng} (\mathbf{N}_{11g} \mathbf{D}_{1g}^{\mathrm{T}} + \mathbf{D}_{1g} \mathbf{N}_{11g}^{\mathrm{T}}) - \mathbf{N}_g \overline{\mathbf{N}}_{1g}^{\mathrm{T}} - \overline{\mathbf{N}}_{1g} \mathbf{N}_g^{\mathrm{T}} - \frac{1}{m_{11g}} (\mathbf{T}_g \overline{\mathbf{T}}_{1g}^{\mathrm{T}} + \overline{\mathbf{T}}_{1g} \mathbf{T}_g^{\mathrm{T}}) \right] \right\} w_g j_g \end{aligned} \tag{A16}$$

where 'GP' indicates that the summation is extended to the Gauss points, subscript g refers to the dependence on the Gauss point coordinate, and w_g and j_g are, respectively, the weight and the jacobian associated to the gth integration point on $\Gamma_{\mathrm{c}0}$.

ACKNOWLEDGEMENTS

The first author gratefully acknowledges the support of the Alexander von Humboldt Stiftung through a 'Humboldt Research Fellowship for Experienced Researchers' for a research stay at the Leibniz Universität Hannover.

DOI: 10.1002/nme

REFERENCES

1. Hughes TJR, Cottrell JA, Bazilevs Y. Isogeometric analysis: CAD, finite elements, NURBS, exact geometry and mesh refinement. *Computer Methods in Applied Mechanics and Engineering* 2005; **194**:4135–4195.
2. Bazilevs Y, Hughes T. NURBS-based isogeometric analysis for the computation of flows about rotating components. *Computational Mechanics* 2008; **43**:143–150.
3. Bazilevs Y, Calo V, Hughes T, Zhang, Y. Isogeometric fluid–structure interaction: theory, algorithms and computations. *Computational Mechanics* 2008; **43**:3–37.
4. Bazilevs Y, Gohean J, Hughes T, Moser R, Zhang Y. Patient-specific isogeometric fluid–structure interaction analysis of thoracic aortic blood flow due to implantation of the Jarvik 2000 left ventricular assist device. *Computer Methods in Applied Mechanics and Engineering* 2009; **198**:3534–3550.
5. Buffa A, Sangalli G, Vazquez, R. Isogeometric analysis in electromagnetics: B-splines approximation. *Computer Methods in Applied Mechanics and Engineering* 2010; **199**:1143–1152.
6. Cottrell JA, Hughes TJR, Bazilevs Y. *Isogeometric Analysis*. Wiley: New York, 2009.
7. Zhang Y, Bazilevs Y, Goswami S, Bajaj C, Hughes T. Patient-specific vascular NURBS modeling for isogeometric analysis of blood flow. *Computer Methods in Applied Mechanics and Engineering* 2007; **196**:2943–2959.
8. Eterovic AL, Bathe KJ. An interface interpolation scheme for quadratic convergence in the finite element analysis of contact problems. *Computational Methods in Nonlinear Mechanics*. Springer: Berlin, New York, 1991; 703–715.
9. Pietrzak G, Curnier A. Large deformation frictional contact mechanics: continuum formulation and augmented Lagrangian treatment. *Computer Methods in Applied Mechanics and Engineering* 1999; **177**:351–381.
10. Padmanabhan V, Laursen T. A framework for development of surface smoothing procedures in large deformation frictional contact analysis. *Finite Elements in Analysis and Design* 2001; **37**:173–198.
11. Wriggers P, Krstulovic-Opara L, Korelc J. Smooth C1-interpolations for two-dimensional frictional contact problems. *International Journal for Numerical Methods in Engineering* 2001; **51**:1469–1495.
12. Krstulovic-Opara L, Wriggers P, Korelc J. A C1-continuous formulation for 3D finite deformation frictional contact. *Computational Mechanics* 2002; **29**:27–42.
13. Stadler M, Holzapfel GA, Korelc J. C^n continuous modelling of smooth contact surfaces using NURBS and application to 2D problems. *International Journal for Numerical Methods in Engineering* 2003; **57**:2177–2203.
14. Landon RL, Hast MW, Piazza SJ. Robust contact modeling using trimmed NURBS surfaces for dynamic simulations of articular contact. *Computer Methods in Applied Mechanics and Engineering* 2009; **198**:2339–2346.
15. Temizer İ, Wriggers P, Hughes TJR. Contact treatment in isogeometric analysis with NURBS. *Computer Methods in Applied Mechanics and Engineering* 2011; **200**(9–12):1100–1112.
16. Laursen TA. *Computational Contact and Impact Mechanics*. Springer: Berlin, 2002.
17. Wriggers P. *Computational Contact Mechanics* (2nd edn). Springer: Berlin, 2006.
18. Zavarise G. Problemi termomeccanici di contatto—aspetti fisici e computazionali, Tesi di Dottorato in Meccanica delle Strutture, Istituto di Scienza e Tecnica delle Costruzioni, Padova, Italy, 1991 (in Italian).
19. Piegl L, Tiller W. *The NURBS Book* (2nd edn). Springer: Berlin, Heidelberg, New York, 1996.
20. Hughes TJR, Reali A, Sangalli G. Efficient quadrature for NURBS-based isogeometric analysis. *Computer Methods in Applied Mechanics and Engineering* 2010; **199**:301–313.
21. Fischer KA, Wriggers P. Frictionless 2D contact formulations for finite deformations based on the mortar method. *Computational Mechanics* 2005; **36**:226–244.
22. Fischer KA, Wriggers P. Mortar based frictional contact formulation for higher order interpolations using the moving friction cone. *Computer Methods in Applied Mechanics and Engineering* 2006; **2006**:5020–5036.
23. Hüeber S, Wohlmuth BI. A primal-dual active set strategy for non-linear multibody contact problems. *Computer Methods in Applied Mechanics and Engineering* 2005; **194**:3147–3166.
24. Puso MA, Laursen TA. A mortar segment-to-segment frictional contact method for large deformations. *Computer Methods in Applied Mechanics and Engineering* 2004; **193**:4891–4913.
25. Puso MA, Laursen TA, Solberg J. A segment-to-segment mortar contact method for quadratic elements and large deformations. *Computer Methods in Applied Mechanics and Engineering* 2008; **197**:555–566.
26. Hesch C, Betsch P. A mortar method for energy-momentum conserving schemes in frictionless dynamic contact problems. *International Journal for Numerical Methods in Engineering* 2009; **77**:1468–1500.
27. Tur M, Fuenmayor FJ, Wriggers P. A mortar-based frictional contact formulation for large deformations using Lagrange multipliers. *Computer Methods in Applied Mechanics and Engineering* 2009; **198**:2860–2873.
28. Hüeber S, Wohlmuth BI. Thermo-mechanical contact problems on non-matching meshes. *Computer Methods in Applied Mechanics and Engineering* 2009; **198**:1338–1350.
29. Nowell D, Hills DA, Sackfield A. Contact of dissimilar elastic cylinders under normal and tangential loading. *Journal of the Mechanics and Physics of Solids* 1988; **36**(1):59–75.
30. Hills DA, Nowell D. *Mechanics of Fretting Fatigue*. Kluwer Academic Publishers: Dordrecht, 1994.
31. Franke D, Düster A, Nübel V, Rank E. A comparison of the h-, p-, hp-, and rp-version of the FEM for the solution of the 2D Hertzian contact problem. *Computational Mechanics* 2010; **45**:513–522.
32. Yang B, Laursen TA, Meng X. Two dimensional mortar contact methods for large deformation frictional sliding. *International Journal for Numerical Methods in Engineering* 2005; **62**:1183–1225.

DOI: 10.1002/nme